Article

Nutrient-sensing alteration leads to age-associated distortion of intestinal stem cell differentiating direction

Zihua Yu[1,2,4], Yuedan Zhu[1,4], Yi Chen[3,4], Chenxi Feng[1,4], Zehong Zhang[1], Xiaoxin Guo[1], Haiou Chen[1], Xingzhu Liu[1], Yu Yuan[1] & Haiyang Chen ®[1] ✉

Nutrient-sensing pathways undergo deregulation in aged animals, exerting a pivotal role in regulating the cell cycle and subsequent stem cell division. Nevertheless, their precise functions in governing pluripotent stem cell differentiation remain largely elusive. Here, we uncovered a significant alteration in the cellular constituents of the intestinal epithelium in aged humans and mice. Employing *Drosophila* midgut and mouse organoid culture models, we made an observation regarding the altered trajectory of differentiation in intestinal stem cells (ISC) during overnutrition or aging, which stems from the erroneous activation of the insulin receptor signaling pathway. Through genetic analyses, we ascertained that the nutrient-sensing pathway regulated the direction of ISC differentiation by modulating the maturation of endosomes and SOX21A transcription factor. This study elucidates a nutrient-sensing pathway-mediated mechanism underlying stem cell differentiation, offering insights into the etiology of stem cell dysfunction in aged animals, including humans.

Nutrient-sensing pathways play a crucial role in the aging process. Restricting dietary intake, for instance, can extend the lifespan of various organisms by deactivating nutrient sensing[1]. Conversely, the impaired regulation of nutrient sensing is commonly observed in elderly humans and patients with age-related conditions like type 2 diabetes (T2D)[2,3]. While the connection between dysregulated nutrient sensing and the aging of individuals is widely acknowledged, many questions remain unknown about the relationship between nutrient sensing and aging.

Adult stem cells are vital for maintaining the stability of tissues and organs by continually generating and replacing fully functional cells[4]. As individuals age, adult stem cells experience deregulation, leading to an inability to sustain the balance in tissues and organs, thereby contributing to age-related diseases. For instance, hair follicle stem cells (HFSCs) in older individuals have a diminished ability to generate new hair shafts, resulting in hair loss[5]. Similarly, muscle satellite cells (MuSCs) in older individuals exhibit a reduced capacity for muscle regeneration following injury, which is a significant factor in the development of sarcopenia[6]. In these cases, significant progress has been made in understanding the mechanisms that regulate stem cell activation and proliferation during the aging process. One common explanation is the energy restriction point within the cell cycle, which appears to be influenced by nutrient sensing[7]. Moreover, nutrient-sensing pathways have been found to impact neural stem cell fate decision[8], human embryonic stem cell differentiation[9], and mesenchymal stem cell differentiation[10]. However, the regulation of nutrient-sensing pathways in stem cell differentiation, especially

[1]West China Centre of Excellence for Pancreatitis and Laboratory of Stem Cell and Anti-Aging Research, Frontiers Science Center for Disease-related Molecular Network, National Clinical Research Center for Geriatrics, West China Hospital, Sichuan University, Chengdu, Sichuan, China. [2]Key Laboratory of Gene Engineering of the Ministry of Education, School of Life Sciences, Sun Yat-sen University, Guangzhou, Guangdong, China. [3]Division of Gastrointestinal Surgery, Department of General Surgery, West China Hospital, Sichuan University, Chengdu, Sichuan, China. [4]These authors contributed equally: Zihua Yu, Yuedan Zhu, Yi Chen, Chenxi Feng. ✉e-mail: chenhy82@scu.edu.cn

the differentiating direction of pluripotent stem cells, in aged animals remains largely unexplored.

Pluripotent stem cells have at least two differentiating directions. As a result, maintaining a balanced differentiation between these two directions is crucial for meeting the tissue's requirements when needed. Failure to maintain this balance, for example in the mammalian hematopoietic system, is associated with myeloproliferative disorders[11] and acute lymphoblastic leukemia[12], which significantly affect body health. A well-known example of functional decline in aging is the mammalian hematopoietic system. This is evidenced by the reduced proliferation potential of hematopoietic stem cells (HSCs) and an elevated ratio of myeloid to lymphoid progenies[13], which subsequently leads to immune system deterioration. Numerous studies have aimed to uncover the mechanisms that regulate the differentiation direction of HSCs during aging[14–17]. However, due to the complex and unstable niche of HSCs[18], investigating these precise mechanisms still presents challenges. Additionally, the understanding of whether other local pluripotent stem cells undergo changes in differentiation direction during aging, and the mechanisms behind these changes, remains limited.

The adult *Drosophila* digestive tract has been established as a simple and useful system for the study of adult stem cell differentiation and aging[19,20]. Furthermore, the nutritional state of *Drosophila* can be easily controlled by manipulating food intake. Similar to the mammalian intestine, the *Drosophila* midgut epithelium is constantly replenished by intestinal stem cells (ISCs)[21,22]. Upon activation, one quiescent ISC can undergo symmetric division to expand the stem cell pool, or asymmetric division to produce a new ISC and a committed progenitor cell called enteroblast (EB), which will further differentiate into a mature polyploid enterocyte (EC)[23]. Occasionally, one ISC can undergo asymmetric division and produce a different type of progenitor cell known as an enteroendocrine mother cell (EMC, also known as pre-EE). The pre-EE subsequently undergoes symmetric division, resulting in the formation of a pair of enteroendocrine (EE) cells that contribute to maintaining homeostasis[24]. High Notch activity is required for ISC to differentiate into EB and also for EB to differentiate into EC. Conversely, under low Notch conditions, the ISC will produce an pre-EE[24]. Studies conducted on the *Drosophila* midgut system have shown that nutrient-sensing pathways play roles in organ development, homeostasis maintenance, and aging[25,26]. It has been demonstrated that insulin receptor (InR) signaling pathway-mediated nutrient sensing regulates ISC proliferation[27]. However, whether InR signaling-mediated nutrient sensing also involves in the ISC differentiation direction remains unknown.

In aged *Drosophila*, ISCs exhibit hyper-proliferation, as indicated by a marked increase in the signal of phosphorylated histone H3 (pH3), a marker of mitotic metaphase[19]. This excessive proliferation is attributed to heightened stress signaling and inflammatory response within the epithelium[28,29]. Additionally, the regulation of ISC-to-EC differentiation becomes disrupted, as evidenced by an elevated ratio of polyploid cells expressing stem cell marker Escargot (Esg)[19]. Aberrant Notch signaling contributes to this dysregulation. A previous study has established a correlation between aging and increased activity of the midgut InR signaling pathway[30]. However, it remains unknown whether the InR signaling pathway plays a role in the regulation of age-related ISC differentiation changes.

In this study, we aimed to investigate the impact of aging on the behavior of intestinal stem cells, specifically in terms of their differentiation direction, in both *Drosophila* and mammals. Our findings demonstrate that ISC differentiation can be altered through an InR signaling pathway-dependent mechanism, acting upstream of the RAB7-SOX21A axis. These results shed light on a novel role for the nutrient-sensing pathway and unveil the underlying mechanism of aging.

Results

The cellular components of the intestine epithelium alter in aged mammals

To explore the influence of aging on the function of the intestine, immunohistochemistry was used to analyze the intestinal epithelium of young and aged individuals. Human digestive tract samples from the control group (age <40) or the elder group (age ≥ 40) were collected. Immunohistochemistry analyses revealed that in human duodenum secretory lineage cells: goblet cells (GCs, marked by Muc2), Paneth cells (PCs, marked by Lyz1), and enteroendocrine cells (EEs, marked by ChgA) were increased in the aged group (Fig. 1a–c, e–g, i–k). Conversely, another kind of epithelial cells, tuft cells (TCs, marked by DCAMKL1), were decreased in the aged group compared to the control group (Fig. 1d, h, l). Similar results were observed in the jejunum, producing consistent findings (Supplementary Fig. 1a–h and Fig. 1m–p). Based on these results, the duodenum was selected as the representative mammalian tissue for further analyses.

To further verify that aging alters the cellular composition of the mammalian intestine epithelium, the intestines of aged mice (18- to 20-month-old) were observed. Immunohistochemistry analyses and alcian blue staining (indicating goblet cells) also demonstrated an increase in goblet cells, Paneth cells, and enteroendocrine cells, as well as a reduction in tuft cells in the duodenum of aged mice (Supplementary Fig. 1i–p and Fig. 1q–t). RT-qPCR test of cell markers revealed elevated expression levels of secretory lineage markers *Gfi1* and *Neurog3*, goblet cell markers *Muc2* and *Tff3*, enteroendocrine cell marker *Chga* was increased in old mice duodenum compared to young mice (Fig. 1u). On the other hand, the expression levels of tuft cell markers *Pou2f3* and *Plcg2* were decreased (Fig. 1u). Notably, the expression level of Paneth cell marker *Lyz* did not show a significant change (Fig. 1u). This may be the final consequence of the increased number of Paneth cells and decreased expression level of Lyz in single Paneth cell[31]. To check the effect of apoptosis in aging, TUNEL staining was performed, revealing no significant change in apoptosis signals in the duodenum of aged mice (Supplementary Fig. 1q–s).

To further investigate the effect of aging on ISCs, organoid culture was employed (see strategy in Supplementary Fig. 1t). Organoids derived from aged mice (18- to 20-month-old) exhibited a decreased survival rate and impaired budding ability (Fig. 1v–x), indicating a functional decline in ISCs with aging. Immunofluorescence staining of Lyz and ChgA revealed an increased presence of PCs and EEs in the aging group compared to the control group (Supplementary Fig. 1u–v and Fig. 1y). RT-qPCR analysis of organoids further confirmed stronger expression of secretory lineage markers in the aging group as compared to the control group (Fig. 1z). Together, these data suggest that aging may affect ISC differentiation direction in the intestine of mammals.
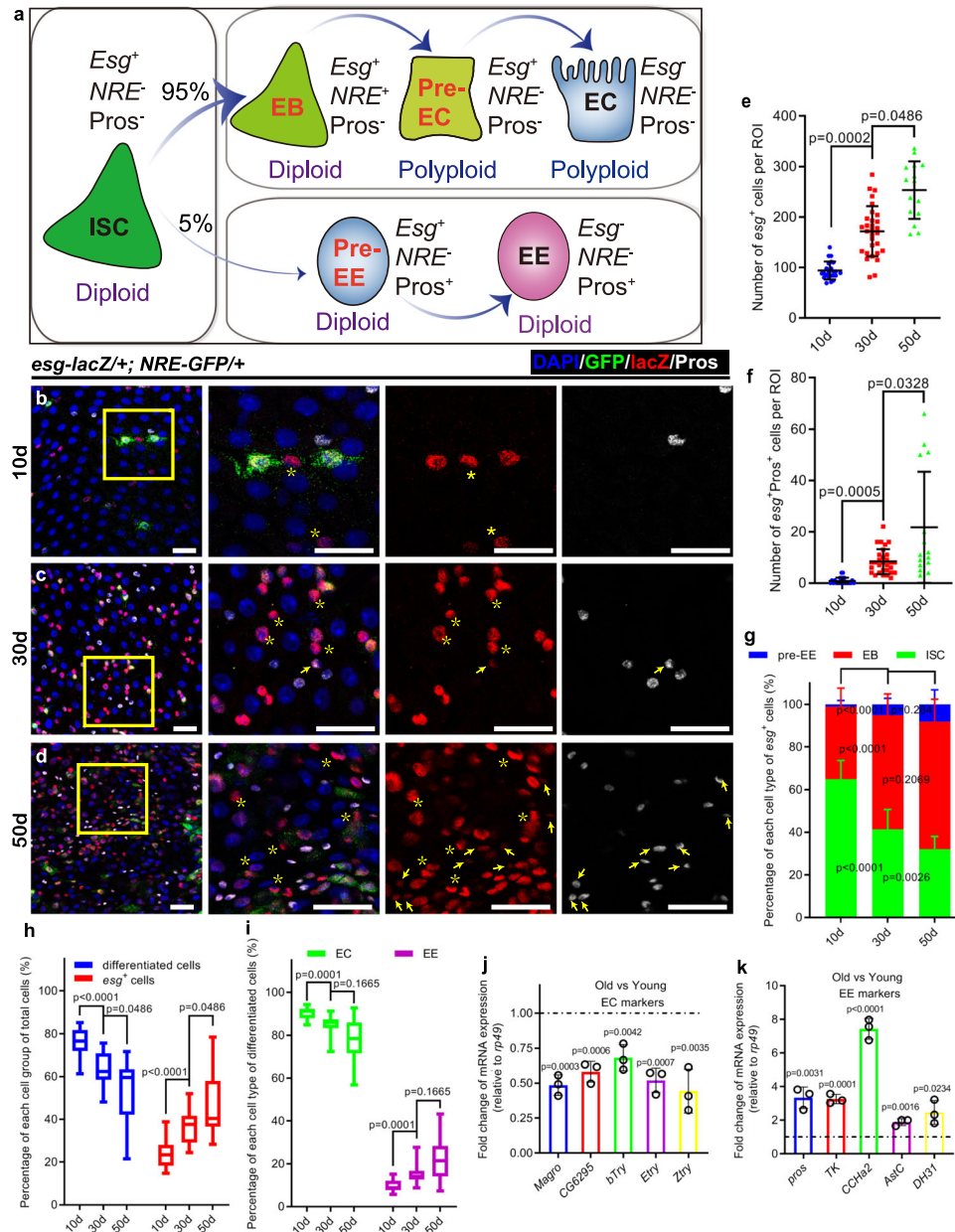
Intestinal stem cell differentiating direction changes upon aging in Drosophila

Compared with the mammalian intestine, *Drosophila* midgut is an ideal model for investigating intestinal stem cell differentiation because of its simpler cellular components, more specific markers, and easier genetic manipulation (Fig. 2a). Using transgenic reporters, *escargot-lacZ* (*esg-lacZ*, indicates ISCs and their differentiating progenies) and *NRE-GFP* (Notch response element-GFP, indicates EBs), along with Prospero (Pros, indicates EEs) antibody staining, we were able to label all kinds of defined epithelial cells in the *Drosophila* midguts. In detail, *esg*-positive *NRE*-negative Pros-negative (*esg*⁺*NRE*⁻Pros⁻) cells, *NRE*⁺ cells, *esg*⁺Pros⁺ cells, *esg*⁻Pros⁺ cells, and *esg*⁻Pros⁻ polyploid cells were recognized as ISCs, EBs, pre-EEs, mature EEs and ECs, respectively (Fig. 2a).

We collected flies at a young age (10 days), middle age (30 days), and old age (50 days) and analyzed the cellular components of their midgut epithelia. Consistent with the previous report[32], our results showed a significant increase in the number of *esg*-lacZ⁺ cells, *NRE*-GFP⁺

Fig. 1 | Aging alters cellular components in the mammalian intestine epithelium. a–h Immunohistochemistry images of human duodenum section from young (**a–d**) and old (**e–h**) group with Muc2 (**a, e**), ChgA (**b, f**), Lyz (**c, g**), and DCAMKL1 (**d, h**) staining. **i–t** Quantification of the percentage of GCs (**i, m, q**), EEs (**j, n, r**), PCs (**k, o, s**) and TCs (**l, p, t**) from the young and old group of human duodenum (**i-l**) and jejunum (**m–p**) section, and mouse duodenum (**q–t**) samples section. $n = 12$ (**i-l**), 8 (**m–p**) and 5 (**q–t**) samples in the young group and $n = 7$ (**i–l**), 5 (**m–p**) and 5 (**q–t**) samples in the old group. **u** The relative mRNA level of indicated marker genes from duodenum tissue of old and young mice. **v–x** Quantification of organoid survival rate (**v**), percentage of organoid with normal function indicated by buds number > 3 (**w**), number of buds per organoid (**x**) and number of PCs or EEs (**y**) at day 7 after seeding. Each dot represents repeating times in (**v–w**) and $n = 9$ in the young group and $n = 10$ in the old group. Each dot represents one organoid in (**x–y**) and $n = 25$ (**x**) and 30 (**y**) in the young group and $n = 30$ (**x**) and 30 (**y**) in the old group. **z** The relative mRNA level of indicated marker genes from organoids derived from old and young mice. Each dot represents the mean value of cell percentage from 5 randomly chosen villi (**i, j, l, m, n, p, q, r** and **t**) or crypts (**k, o, s**) in each section. The mRNA level of each gene from young mice was normalized to 1 and each experiment was repeated for 3 times in (**u**) and (**z**). Scale bar, 100 μm. Red arrows indicate cells with positive signals. Bars are mean ± SD. Statistics were measured by two-tailed, unpaired student's *t*-tests. Source data are provided as a Source Data file. Individual-level data as well as gender and age of human participants are provided in this file.

Fig. 2 | Aging alters intestinal stem cell differentiating direction in *Drosophila*. **a** A model of cell lineage in *Drosophila* midgut epithelium and the characteristic marker for each cell type was indicated. **b**–**d** Representative immunofluorescence of midguts with GFP (green), lacZ (red), and Pros (white) staining from 10d (**b**), 30d (**c**), and 50d (**d**) flies (*esg-lacZ/+; NRE-GFP/+*). **e, f** Quantification of the number of *esg*+ cells (**e**) and *esg*+Pros+ cells (**f**) per region of interest (ROI) of midguts in experiments (**b**–**d**). **g** The percentage of ISCs, EBs, and Pre-EEs to *esg*+ cells of midguts in experiments (**b**–**d**). **h** The percentage of differentiated cells and *esg*+ cells to total cells of midguts in experiments (**b**–**d**). **i** The percentage of ECs and EEs to total differentiated cells of midguts in experiments (**b**–**d**). **j, k** The relative mRNA

expression level of EC-specific genes (**j**) and EE-specific genes (**k**) from whole midgut in old flies compared with young flies. The mRNA expression level of each gene from young flies was normalized to 1. Each experiment was repeated for 3 times. ROI size 84,100 µm2. DAPI-stained nuclei (blue). Yellow asterisks indicate *esg*+*NRE*-Pros- ISCs. Yellow arrows indicate *esg*+Pros+ Pre-EE. Scale bar, 25 µm. For dot plots and (**g**), bars are mean ± SD. For box plots, box shows median, 25th and 75th percentiles and whiskers represent minima and maxima. Statistics were measured by one-way ANOVA in (**e**–**i**) and two-tailed, unpaired Student's *t*-test in (**j, k**). Each dot represents one ROI in (**e, f**). $n = 23$, 30 and 15 in 10d, 30d, and 50d group, respectively in (**e**–**i**). Source data are provided as a Source Data file.

cells, and Pros+ cells in *Drosophila* midguts during aging (Fig. 2b–e and Supplementary Fig. 2a), This finding indicates that ISCs suffer dysregulation of proliferation and differentiation with age. Interestingly, marking ISCs with *esg*+*NRE*Pros- just exhibited a mild increase in ISC number (Supplementary Fig. 2a), not as that dramatic increase as marking ISCs with Delta (Dl)[32]. We propose that the substantial increase in Dl+ cells in aged *Drosophila* midguts may not solely comprise ISCs but mainly include under-differentiated progenitor cells that fail to eliminate the expression of Dl during aging. In fact, the number of ISCs does not undergo such a significant increase in the aged

mammalian intestine[20]. Therefore, we believe that our strategy for labeling and quantifying ISCs in *Drosophila* upon aging may be more reasonable. When applying our labeling and quantification approach to aging *Drosophila*, the proportion of *esg*+*NRE*Pros- labeled ISCs among *esg*+ cells showed a significant decrease with age (Fig. 2g). This result is consistent with the decline of ISCs rate observed in aging mammalian intestines[20], indicating a decrease in ISC differentiation function during aging. Simultaneously, the number of pre-EEs and their percentage among *esg*+ cells increased in old flies compared to young flies (Fig. 2b–d, f, g). Furthermore, we observed a decreased

percentage of mature terminal differentiated cells (mature EEs and ECs, namely *esg*⁻ cells) decreased with aging (Fig. 2h), which suggested a functional decline of intestines in aged *Drosophila*.

Notably, the number of ECs increased in 30-day-old flies but then decreased in 50-day-old flies (Supplementary Fig. 2a). This number rose in 30-day-old flies because of the smaller room of each cell that was caused by the gut epithelia wrinkling during aging. Thus, more ECs were counted in one region of interest (ROI) (Fig. 2b–d). The number of ECs dropped in 50-day-old flies because most of the gut epithelial cells became *esg*⁺ at this age (Fig. 2d). Then we counted ECs number per 100 total cells and observed an obvious decrease trend (Supplementary Fig. 2b). This suggested reduced function of ECs. Importantly, we noticed that, while the number of mature EEs (*esg*⁻Pros⁺) and their percentage in differentiated cells significantly increased in old flies compared to young flies (Supplementary Fig. 2a and Fig. 2i), the percentage of mature ECs (*esg*⁻ polyploid cells) significantly decreased (Supplementary Fig. 2a and Fig. 2i). To test the potential for the shift in the function of ECs and EEs in aged *Drosophila* midguts, we performed RT-qPCR on the whole midgut and detected the expression level of several enzymes expressed in ECs and hormone peptides secreted by EEs. The results showed that the expression levels of these EC-specific enzymes significantly decreased in old flies compared to young flies (Fig. 2j), while the expression level of these EE-secreted hormones dramatically increased (Fig. 2k). All these data reveal that ISCs suffer deregulated differentiating direction and the midguts exhibit functional change upon aging.

Lineage tracing is a widely used method to investigate stem cell differentiation[33]. In *Drosophila*, lineage tracing is switched on by changing the culture temperature, activating the transgenic heat shock promotor or Gal4 transcription factor, followed by the action of the recombinase Flippase[34]. We used two lineage tracing systems, mosaic analysis with a repressive cell marker (MARCM)[35] and G-Trace[36], to investigate ISC differentiation. However, neither of them could provide convincing data because of non-negligible leaky expression in old flies (Supplementary Fig. 2c, d).

Down-regulation of the activity of the InR signaling pathway restores the change of ISC differentiation direction upon aging

The process of aging often involves the disruption of nutrient-sensing pathways[3]. To investigate the possible role of nutrient-sensing pathways in the age-related changes in intestinal stem cell differentiation in the *Drosophila* midgut, the expression of phosphorylated Akt (pAkt), phosphorylated 4E-BP (p4EBP) and tGPH was detected. Akt is a vital downstream member of insulin receptor and 4E-BP is a well-known substrate of mechanistic target of TOR signaling pathway. tGPH is a GFP reportor monitering PIP₃ distribution[37]. They serve as commonly used indicator of nutrient-sensing pathway activity[38,39]. To assess the fidelity of these reporters in representing InR activity within intestinal cells, we activated InR signaling in *esg*⁺ cells by overexpression of *InR*^{CA}. Our findings revealed a substantial elevation in tGPH and pAkt levels in Dl⁺ cells relative to controls (Supplementary Fig. 3a–c). Then we analyzed tGPH and pAkt, p4EBP levels in both young and old ISCs. Notably, tGPH expression was subdued in young Dl⁺ cells but exhibited an increase in the aged cohort (Supplementary Fig. 3d–e). pAkt level is significantly up-regulated in Dl⁺ cells (Fig. 3a–c) or *esg*⁺*NRE*⁻ cells (Supplementary Fig. 3f, g and j) in old flies compared to their younger counterparts. In young flies, p4EBP was scarcely detected in young *esg*⁺*NRE*⁻ cells, whereas its expression was intensified in *esg*⁺*NRE*⁻ cells within the aged group (Supplementary Fig. 3l, m). This indicated that the activity of the insulin receptor signaling pathway is upregulated in ISCs during natural aging. In consistant with this, pH3 staining revealed more mitotic cells in the midgut during aging (Supplementary Fig. 3n). We also observed pAkt level in ECs but found no elevation in aged group (Supplementary Fig. 3k), which is intriguing and may be related to insulin resistance in ECs.

Insulin receptor (InR) is a widely investigated nutrient sensor and is reported to activate during aging[26,40]. InR signaling pathway has been reported to regulate ISC proliferation[27]. However, it is unclear whether InR signaling pathway plays a role in the regulation of aging-mediated change of ISC differentiation direction. To test this, *chico*⁺/⁻ heterozygote mutant was introduced, in which the activity of the InR signaling pathway is genetically reduced by manipulating the expression of *chico*, an insulin receptor substrate commonly used in *Drosophila* research[41]. The pAkt level were down-regulated in *esg*⁺*NRE*⁻ cells of old *chico*⁺/⁻ heterozygote mutants compared to old wild-type flies (Supplementary Fig. 3g, h, j). Thus, we checked the cellular components of the intestinal epithelia in *chico*⁺/⁻ heterozygote mutants. As expected, we found no differences between the wild type and this heterozygote mutant at a young age (Fig. 3d, e, g–j). In old flies, the wild-type group exhibited the following alterations: (1) an increased number of *esg*⁺ cells (Fig. 3d, g); (2) an increased pre-EE proportion among *esg*⁺ cells (Fig. 3d, h); (3) a decreased ratio of differentiated cells among total epithelial cells (Fig. 3d, i); (4) a decreased mature EC ratio among the differentiated cells (Fig. 3d, j); and (5) an increased number of pH3⁺ cells in the midguts (Supplementary Fig. 3n). Remarkably, these phenotypes were rescued in the *chico*⁺/⁻ heterozygote mutant group (Fig. 3e, g–j, Supplementary Fig. 3n). These results provide evidence that the InR signaling pathway is involved in regulating the direction of ISC differentiation during the aging process.

Dietary restriction (DR) is a well-established approach for promoting healthy aging, and its mechanism is understood to involve the modulation of nutrient-sensing pathways[42]. In *Drosophila*, DR has been shown to play a crucial role in extending lifespan[43]. In this study, we found that DR down-regulated pAkt level in *esg*⁺*NRE*⁻ cells of aged flies (Supplementary Fig. 3g, i, j). Then, DR significantly attenuates not just the increase of *esg*⁺ cell number but also the increase of pre-EE ratio in intestinal epithelia of aged *Drosophila* (Fig. 3f–h). Moreover, DR restored the decrease of the proportion of differentiated cells among the total intestinal epithelial cells (Fig. 3i) and rescued the ratio of mature ECs among the differentiated cells (Fig. 3j) in midguts of aged *Drosophila*. Also, DR reduced the increased pH3⁺ cells in the aged midguts (Supplementary Fig. 3n). Since the DR-treated *Drosophila* showed a similar alleviation of age-associated ISC differentiation defects as observed in the *chico*⁺/⁻ heterozygote mutant flies (Fig. 3e–j, Supplementary Fig. 3n), this again highlights the significant impact of downregulating nutrient-sensing pathways on delaying intestinal stem cell aging.

To check the conservation of evaluation of insulin signaling pathway in ISCs, we tested the level of p4EBP protein in mouse small intestine crypts via western blot analysis. Results revealed the same trend in mammals and *Drosophila* (Supplementary Fig. 4a).

Overnutrition leads to the change of intestinal stem cell differentiating direction

Previous reports point out that the overnutrition mediated by high sugar diet (HSD) induces an expansion of Dl⁺ ISCs in *Drosophila*, a similar phenotype to that observed during aging[44]. However, it remains unknown whether overnutrition affects the differentiating direction of ISCs. To investigate ISC behavior under overnutrition conditions, we collected 5-day-old flies and fed them with HSD, methionine, leucine or normal food (NF) for another 5 days (Fig. 4a). The findings revealed a significant upregulation of both both pAkt (Supplementary Fig. 4b–f) and p4EBP (Supplementary Fig. 4g–j) in *esg*⁺*NRE*⁻ cells following HSD, methionine or leucine supplementation. These observations indicate that HSD, methionine, and leucine supplementation induced alterations in nutrient sensing pathways, ultimately leading to *Drosophila* overnutrition. Subsequently, we conducted statistical quantification of all specified cell types under HSD, methionine, or leucine supplementation. Overnutrition led to an increase in *esg*-lacZ⁺ cells (Fig. 4b, c, f and Supplementary Fig. 5a–c), predominantly comprising EBs and
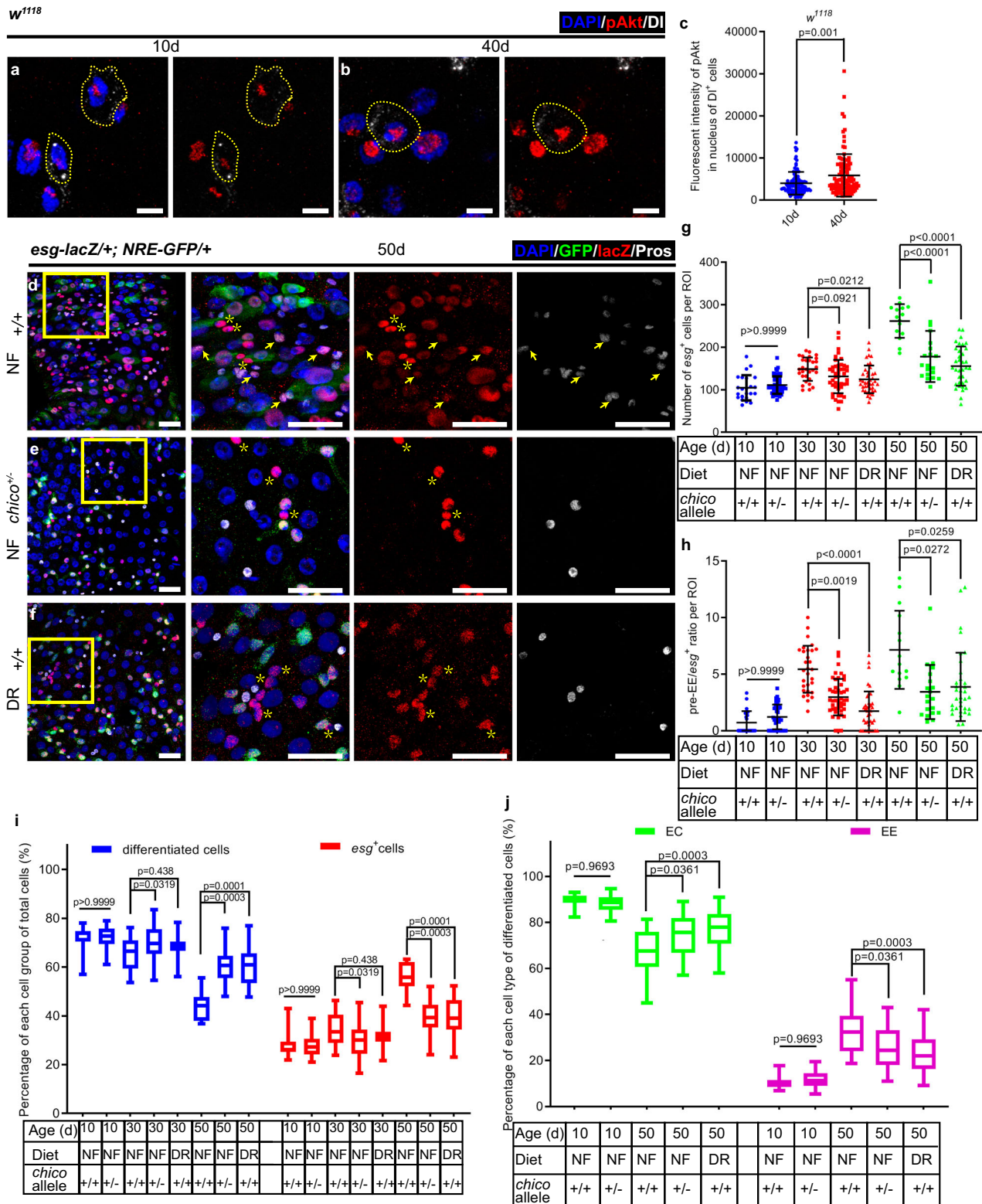
pre-EEs but not ISCs (Supplementary Fig. 5d–f and h). Moreover, overnutrition increased the percentage of pre-EEs among *esg*+ cells in *Drosophila* midguts (Fig. 4b, c, g and Supplementary Fig. 5a–c, i). This indicated that, besides of ISC proliferation rate, overnutrition also regulates ISC differentiating direction. Furthermore, we found that overnutrition led to a dramatic decrease in the percentage of differentiated cells in intestinal epithelia (Fig. 4h and Supplementary Fig. 5j), but had no or mild effect on the percentage of ECs or EEs among differentiated cells (Supplementary Fig. 5g, k).

Next, we tested whether the *chico*+/– heterozygote mutant could mitigate the ISC aging phenotypes. We found that *chico*+/– flies fed with NF exhibited no differences in the cellular components of the intestinal epithelium compared to wild-type flies fed with NF (Fig. 4b, d, f–h and Supplementary Fig. 5d–f). When fed with HSD, while the percentages of *esg*+ cells (undifferentiated cells) and *esg*+Pros+ cells (pre-EEs) increased in the midguts of the wild-type flies (Fig. 4c, f–h and Supplementary Fig. 5f), they remained unchanged in the midguts of the *chico*+/– flies (Fig. 4e, f–h and Supplementary Fig. 5f). These data

Fig. 3 | The InR signaling pathway is responsible for ISC aging phenotype.
a, **b** Immunofluorescence of midguts with pAkt (red) and Dl (white) staining from 10d (**a**) and 40d (**b**) w^{1118} flies. **c** Quantification of the fluorescence intensity of pAkt in nuclear of Dl-labeled ISCs of midguts in experiments (**a**, **b**). Each dot represents one ISC and $n = 103$ in 10d group and $n = 105$ in 40d group. **d**–**f** Representative immunofluorescence of midguts with GFP (green), lacZ (red) and Pros (white) staining from 50d control flies raised on normal food (**d**), 50d $chico^{-/+}$ flies raised on normal food (**e**), and 50d flies raised on dietary restriction (DR)-food (**f**). Flies carrying *esg-lacZ/+; NRE-GFP/+* were used as control. Asterisks indicate $esg^+NRE^-Pros^-$ ISCs. Arrows indicate esg^+Pros^+ Pre-EEs. **g** Quantification of the number of esg^+ cells per ROI with indicated genotypes and treatments. ROI size 84,100 μm^2. **h** The ratio of Pre-EE to total esg^+ cells per ROI with indicated genotypes and treatments. **i** The percentage of differentiated kinds of cells and esg^+ cells to total cells with indicated genotypes and treatments. **j** The percentage of ECs and EEs to total differentiated cells with indicated genotypes and treatments. DAPI-stained nuclei (blue). Yellow frames indicate Dl-labeled ISCs. Yellow asterisks indicate $esg^+NRE^-Pros^-$ ISCs. Yellow arrows indicate esg^+Pros^+ Pre-EE. Scale bar, 5 μm in (**a**, **b**) and 25μm in (**d**–**f**). For dot plots, bars are mean ± SD. For box plots, box shows median, 25th and 75th percentiles and whiskers represent minima and maxima. Statistics were measured by one-way ANOVA. From left to right, $n = 23, 48, 30, 45, 40, 15, 20$, and 35, respectively in (**g**–**i**). Each dot represents one ROI in (**g**, **h**). **j** shares the same n number with (**g**–**i**) in indicated groups. Source data are provided as a Source Data file.

suggest that HSD-induced overnutrition affects ISC differentiation direction through an InR signaling-dependent mechanism.

Furthermore, we examined whether activation of InR signaling pathway in ISCs alone is sufficient to induce the change of ISC differentiation direction. We used ISC specific-Gal4 (*NRE-lacZ; esg-gal4, UAS-GFP, GBE-gal80; tub-gal80^{ts}*, namely ISC^{ts}) to upregulate the activity of InR (Supplementary Fig. 6a) by (1) force expression of a constitutively active version of InR (*InR^{CA}*), (2) knockdown of repressive ligand insulin-like peptide 6 (*Ilp6*), or (3) knockdown of intrinsic repressor Phosphatase and tensin homolog (*Pten*). The results demonstrated that all of these manipulations in young flies (except for depletion of *Pten*) had little effect on $esg^+NRE^-Pros^-$ ISCs (Fig. 4i), and led to an increase of EBs (Fig. 4j) and esg^+Pros^+ pre-EEs (Fig. 4k and Supplementary Fig. 6b–d), and a decrease in differentiated cells (Supplementary Fig. 6e), but did not affect the percentage of ECs or EEs among differentiated cells (Supplementary Fig. 6f). On the other hand, we down-regulated the activity of InR by (1) force expression of a dominant negative version of InR (*InR^{DN}*), (2) knockdown of *chico*, or (3) knockdown of InR. As an initial assessment, we initially evaluated these interventions in young flies and noted no disparities in any of the assessed outcomes (Fig. 4i–k and Supplementary Fig. 6d–f). In old *Drosophila* (see the strategy in Supplementary Fig. 6g), as expected, while the control group exhibited a higher ISC number, EB number, pre-EE number, pre-EE ratio, and decreased differentiated cells and percentage of ECs among differentiated cells, down-regulation of InR signaling rescued these changes (Fig. 4l–o and Supplementary Fig. 6h–m). Also, down-regulation of InR signaling reduced the high pH3$^+$ cell number in aged midguts (Supplementary Fig. 6n).

To further elucidate the involvement of InR signaling in the regulation of ISC differentiation, we utilized G-Trace (Supplementary Fig. 7) and MARCM (Supplementary Fig. 8) to trace the lineages of ISCs with both upregulated and downregulated InR signaling activity. Our results revealed that clones with heightened InR signaling activity (via overexpression of *InR^{CA}*, depletion of *Pten*, or treatment with HSD) encompassed a greater number of cells and EEs (Supplementary Fig. 7a–d, g, and h and Supplementary Fig. 8a–d, g, h). Conversely, HSD treatment in clones with reduced InR signaling activity (via overexpression of *InR^{DN}*) did not lead to an increase in clone size or EE number (Supplementary Figs. 7e–h and 8e–h). Dl staining in clones revealed that among these manipulations or HSD treatment, only depletion of *Pten* reduced the number of ISCs per clone (Supplementary Fig. 7i–k and Supplementary Fig. 8i–k). In conjunction with the observations in *ISC^{ts}>Pten RNAi* (Fig. 4), these findings indicated the presence of other unidentified effects related with cell identity resulting from *Pten*. This supposition is bolstered by reports with *Pten* depletion focused on B cells[45] and HSCs[46]. Furthermore, clones treated with HSD consisted of more EBs and EEs, with a robust increase in EEs (Supplementary Fig. 8l–n).

Subsequently, to delve deeper into the role of InR signaling in other cell types during age-related alterations, we implemented manipulations with EB-specific *NRE^{ts}-Gal4* or EC-specific *Mex-Gal4* (Supplementary Fig. 9). The findings indicated that the activation of InR signaling in EBs, but not ECs, partially mirrored these age-related changes (Supplementary Fig. 9a, b, e–j, m, n). Furthermore, inhibiting InR signaling in EBs but not ECs mitigated these age-related changes (Supplementary Fig. 9c–h, k–n).

Together, these data provide evidence that overnutrition and aging-mediated elevated activity of the InR signaling pathway leads to a shift in the differentiating direction of intestinal stem cells.

RAB7-mediated endocytosis functions in the regulation of age-associated change of ISC differentiation direction

To elucidate the mechanisms underlying the disruption of ISC differentiation direction caused by increased InR signaling in aged *Drosophila*, we conducted a targeted genetic screen using ISC^{ts}-Gal4 to manipulate the expression of genes known to regulate ISC behaviors during aging. The selected genes were predominantly chosen based on their involvement in pathways such as mTor signaling, Notch signaling, JAK/STAT signaling, EGFR signaling, TGF-β signaling, autophagy, endocytosis[20,47–50], as well as genes previously implicated in stem cell aging and differentiation, such as *escargot*[51] and *parkin*[52]. We aimed to identify genes that can both induce a similar ISC differentiation direction change in young *Drosophila* (see the strategy in Supplementary Fig. 10a and representative immunofluorescence images are shown in Supplementary Fig. 10b–m) and restore the ISC differentiation direction defect in aged *Drosophila* (see the strategy in Supplementary Fig. 10p and the representative immunofluorescence images are shown in Supplementary Fig. 10q–y and Supplementary Fig. 11a–d).

In young *Drosophila*, we did not find a significant change in the number of ISCs ($esg^+NRE^-Pros^-$ cells) under these genetic manipulations, except in the case of Notch depletion (Fig. 5a). This observation aligns with the findings in the wild-type reporter flies (Supplementary Fig. 2a). NRE^+ EB cells were increased by depleting RAB7 or by overexpressing EGFR (Fig. 5b). Pre-EE number and their ratio among esg^+ cells was increased by several means: (1) downregulating Notch signaling through Notch depletion; (2) impairing the endocytosis process via RAB7 depletion (a small G protein responsible for late endosome formation); (3) depletion of Escargot; or (4) upregulating EGFR signaling through overexpression of EGFR (Fig. 5c and Supplementary Fig. 10n). In addition, a decrease of differentiated cells (esg^- cells) was found in flies with Notch or RAB7 depletion or EGFR overexpression, but not in flies with Escargot depletion (Fig. 5d). Finally, these manipulations hardly changed the percentage of ECs or EEs among differentiated cells (Supplementary Fig. 10o).

In aged *Drosophila*, we observed that the aging-related defects in ISC behavior, encompassing changes in ISC number (Fig. 5e), EB number (Fig. 5f), the ratio of pre-EE among esg^+ cells (Fig. 5g), and the ratio of differentiated cells (Fig. 5h) were restored by various interventions. These interventions included: (1) enhancing Notch signaling activity via *Notch* overexpression or knocking down *asense* (*ase*); (2) overexpression of Sox21A, a SOX family transcription factor involved in ISC-to-EC differentiation[53,54]; (3) suppressing JAK/STAT signaling activity through the depletion of *domeless* (*dome*, receptor of JAK/STAT signaling); (4) inhibiting EGFR signaling activity through the
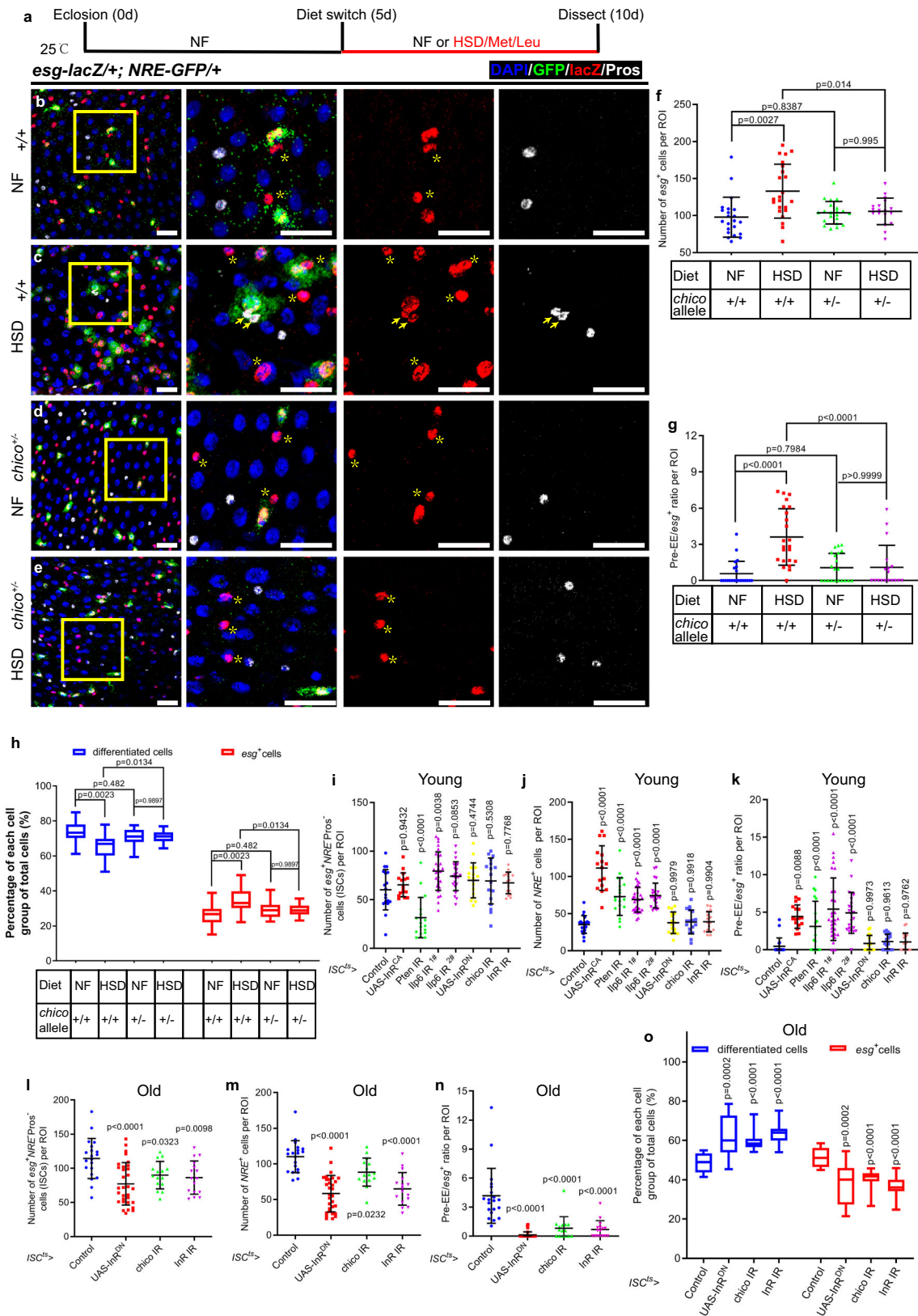
force expression of a dominant negative form of *EGFR* (*EGFR*^{DN}); (5) overexpressing Escargot; (6) promoting autophagy through *TSC1* overexpression; and (7) enhancing endocytosis via the force expression of a constitutive active form of RAB7 (RAB7^{CA}) (Fig. 5e–h). However, the defects related to a higher percentage of mature EEs and a lower percentage of mature ECs in aging individuals were only rescued

by the overexpression of (1) Notch, (2) Escargot, and (3) RAB7^{CA}, and overexpression of SOX21A exhibit obvious trend of rescue (Fig. 5i). Notably, manipulating the TGF-β pathway through depletion or overexpression of the transcription factor mad, knocking down receptor thickveins (tkv), or overexpressing its constitutively active form (tkv^{CA}) did not affect ISC behavior in either the young or aged groups

Fig. 4 | Overnutrition alters intestinal stem cell differentiating direction via InR signaling pathway. a Diagram of the experimental procedure of fly treatment. **b**−**e** Immunofluorescence images of midgut with *esg*-lacZ (red), *NRE*-GFP (green), and Pros (white) staining from control flies (*esg-lacZ/+; NRE-GFP/+*) cultured in NF (**b**), flies cultured in HSD (**c**), *chico*^{+/−} flies cultured in NF (**d**) and *chico*^{+/−} flies cultured in HSD (**e**). **f**, **g** Quantification of the number of *esg*^{+} cells (**f**) and the ratio of Pre-EE cells to *esg*^{+} cells per ROI (**g**) with indicated genotypes and food treatments of midguts in experiments (**b**-**e**). **h** The percentage of differentiated cells and *esg*^{+} cells to total cells in indicated genotypes and food treatments of midguts in experiments (**b**-**e**). **i**, **j** Quantification of the number of *esg*[+]*NRE*⁻Pros⁻ ISCs (**i**) and *NRE*[+] EBs (**j**) per ROI with indicated genotypes of midguts in young *Drosophila*. **k** The ratio of Pre-EE cells to *esg*^{+} cells per ROI with indicated genotypes of midguts in young *Drosophila*. **l**, **m** Quantification of the number of *esg*[+]*NRE*⁻Pros⁻ ISCs (**l**) and *NRE*[+] EBs (**m**) per ROI with indicated genotypes of midguts in old *Drosophila*. **n** The ratio of Pre-EE cells to *esg*^{+} cells per ROI with indicated genotypes of midguts in old *Drosophila*. **o** The percentage of differentiated cells and *esg*^{+} cells to total cells in indicated genotypes of midguts in old *Drosophila*. DAPI-stained nuclei (blue). ROI size 84,100 μm². Yellow asterisks indicate *esg*[+]*NRE*⁻Pros⁻ ISCs. Yellow arrows indicate *esg*[+]Pros[+] Pre-EE. Scale bar, 25 μm. For dot plots, bars are mean ± SD. For box plots, box shows median, 25th and 75th percentiles and whiskers represent minima and maxima. Each group was compared to the control group in (**i**-**o**). Statistics were measured by one-way ANOVA. Each dot represents one ROI in (**f**, **g**) and (**i**-**n**). From left to right, *n* = 22, 19, 21 and 18, respectively in (**f**-**h**); *n* = 18, 19, 35, 23, 16, 17, 17 and 16, respectively in (**i**-**k**); *n* = 20, 31, 15 and 16, respectively in (**l**-**o**). Source data are provided as a Source Data file.

(Fig. 5a−d, Supplementary Figs. 10j−m and 11a−i). This suggests that the TGF-β pathway may not be involved in ISC aging.

InR signaling and TOR signaling are vital nutrient-sensing pathways. A previous report uncovered that in embryonic stem cells (ESCs), disruption of InR signaling reduced mTOR activity, leading to impaired ESC proliferation and differentiation[55]. Consistent with this, we explored whether InR signaling regulated ISC differentiation direction through TOR signaling (Supplementary Fig. 12a-f). Notably, we discovered that the phenotypic changes in ISC differentiation caused by overexpression of *InR*[CA], including the increase of the number of EB cells, pre-EE cells and their ratio in *esg*^{+} cells, as well as the decrease of differentiated cells among total epithelial cells, were significantly restored by knock-down of *mTOR* or treatment with rapamycin (Supplementary Fig. 12h-k), while the number of ISCs and the percentage of ECs among differentiated cells remainde unchanged (Supplementary Fig. 12g, l). This suggested that TOR signaling functions downstream of the InR signaling to regulate ISC differentiation.

Since the Notch signaling pathway has been well established as a regulator of ISC differentiation, our objective was to investigate the genetic relationship between the InR signaling pathway and the Notch signaling pathway (Supplementary Fig. 13a-d). Similar to the depletion of mTOR, the overexpression of the intracellular domain of Notch (*Notch*[Intra]) was capable of restoring the phenotypic changes in ISC differentiation caused by overexpression of *InR*[CA] (Supplementary Fig. 13e-j). This suggested that Notch signaling pathway functions downstream of the InR signaling to regulate ISC differentiation. This observation suggests that the Notch signaling pathway operates downstream of the InR signaling pathway in the regulation of ISC differentiation. Given that the function of the Notch signaling pathway has already been reported, we did not further focus on it.

These data suggested a correlation between intrinsic signaling pathways and aging-related phenotypes in intestinal stem cells. Among these signaling and cellular processes, only manipulation of RAB7-mediated endocytosis activation induced similar changes in ISC differentiation direction in young *Drosophila* and restored the defective ISC differentiation direction in aged *Drosophila* (Fig. 5a-i). Thus, we predicted that RAB7 and its mediated endocytosis may function downstream of InR signaling in regulating ISC differentiation direction changes during aging in *Drosophila*.

InR signaling pathway functions upstream of the RAB7-SOX21A axis to regulate age-associated intestinal stem cell differentiation change
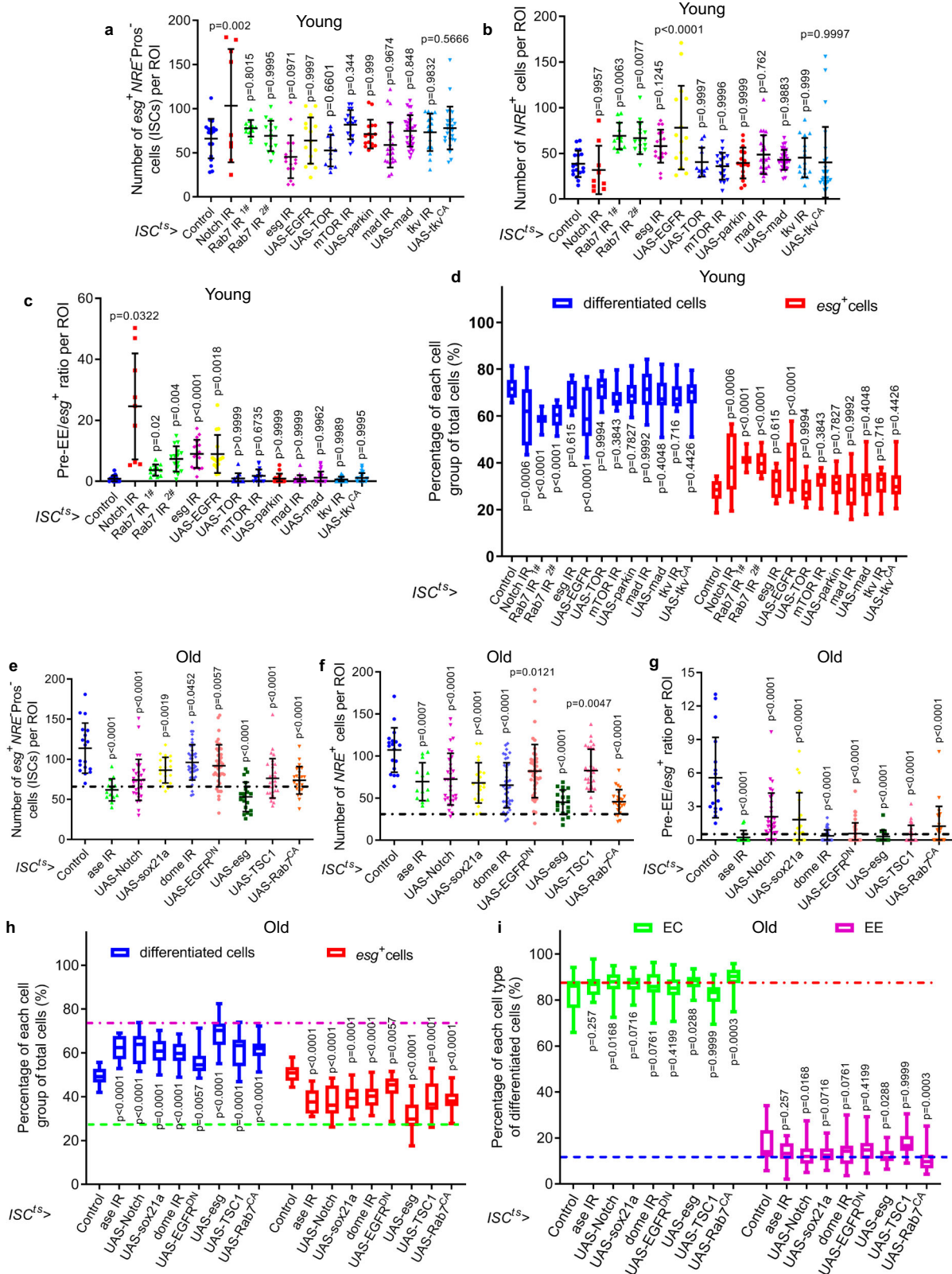
Next, we investigated the genetic relationship between InR signaling and RAB7-mediated endocytosis in the regulation of ISC differentiation direction. Using UAS-RAB7-GFP reportor, we observed a reduction in the expression of RAB7 in Dl^{+} cells upon activation of InR signaling through overexpression of *InR*[CA] driven by *esg*-Gal4 (Supplementary Fig. 14a−c). Futhermore, DR up-regulated RAB7 level in *esg*[+]*NRE*⁻ cells of aged midgut compared to aged controls (Supplementary Fig. 14d−f). Notably, we discovered that the phenotypic changes in ISC

differentiation caused by overexpression of *InR*[CA], including of the number of EB cells, pre-EE cells and their ratio in *esg*^{+} cells, and the decrease of differentiated cells among total epithelial cells, were significantly restored when RAB7[CA] was forcibly expressed driven by *ISC*[ts]-*Gal4* (Fig. 6a−d and f−i), while the number of ISCs and the percentage of ECs among differentiated cells remainde unchanged (Fig. 6e, j). This suggested that RAB7 functions downstream of the InR signaling to regulate ISC differentiation.

Recently, we have reported a mechanism of ISC-to-EC differentiation mediated by the RAB7-SOX21A axis[56] and observed the downregulation of RAB7 expression in ISCs of aged *Drosophila*[57]. In addition, previous research indicates that Dl[+] ISC differentiation direction is regulated by the negative feedback loop of the Scute (Sc) molecule[58]. Therefore, it is plausible to hypothesize that the increased ISC-to-EE differentiation in aged *Drosophila* midguts may arise from impairment of the RAB7-SOX21A axis, leading to reduced ISC-to-EC differentiation during aging. Consequently, the misregulation of ISC differentiation direction in aged *Drosophila* midguts may be caused by the downregulation of the RAB7-SOX21A axis, which in turn results in a failure of ISC-to-EC differentiation and subsequently affects the Sc feedback loop to promote ISC-to-EE differentiation.

To test this hypothesis, we first checked the expression of SOX21A in EBs of young and aged *Drosophila*. A previous report highlighted the robust expression and predominant function of SOX21A in EBs, contrasting with its weak expression in Dl[+] ISCs[54]. We previously generated an endogenous SOX21A-HA reporter line by CRISPR/Cas9[56], which can report the endogenous cellular SOX21A expression. Combined with the *NRE*-GFP reporter, we investigated the endogenous expression of SOX21A in EB cells under stress and/or aging conditions. Results showed that SOX21A was up-regulated after bleomycin treatment in young flies (Fig. 7a, c, e). However, in aged flies, SOX21A exhibited lower intensity in EB cells (Fig. 7a, b, e), and it was not up-regulated by bleomycin treatment (Fig. 7b, d, e). These data are intriguing because it is accepted that aging is viewed as a form of chronic stress for stem cells[59]. Together, we demonstrate that SOX21A is abnormally down-regulated in EBs during aging.

While previous studies have reported the accumulation of EBs in young flies upon SOX21A depletion in *esg*^{+} cells[53], it remains unclear whether the disruption of SOX21A also leads to a secondary effect of pre-EE (*esg*[+]Pros^{+} cells) accumulation in the *Drosophila* midgut. To address this, we depleted SOX21A both in *esg*^{+} cells using *esg*[ts]-Gal4 and in specifically ISCs using ISC[ts]-Gal4 and only observed an increase in the ratio of pre-EEs among *esg*^{+} cells compared to control flies in *esg*[ts]-Gal4-driven manipulation (Supplementary Fig. 15a−d), but not in ISC[ts]-Gal4-dirven manipulation (Fig. 7f, g, m). Meanwhile, the depletion of SOX21A in ISCs did not affect ISC number, EB number, the percentage of differentiated cells among total epithelial cells, or the percentage of ECs among differentiated cells (Fig. 7k, l, n and Supplementary Fig. 15o). These combined data suggested that the age-associated down-regulation of SOX21A in EBs contributes to the increase of ISC-to-EE differentiation in aged *Drosophila* midguts.

Furthermore, we examined the genetic relationship between the InR signaling pathway and SOX21A in the regulation of ISC differentiation direction. We first tested the expression of SOX21A in EBs with either upregulated or downregulated InR signaling activity. In young flies, we observed a reduction in the expression of SOX21A in EBs when InR signaling was activated by treatment of HSD or overexpression of InR^{CA} (Supplementary Fig. 15e, f, i, j, k, n). Conversely, the expression of SOX21A in EBs was up-regulated in old flies when InR signaling was inhibited by treatment of DR or overexpression of InR^{DN} (Supplementary Fig. 15g, h, l, m). Then, similar to RAB7, we found that forced expression of SOX21A by ISC^{ts}-Gal4 significantly restored the phenotypic changes in ISC differentiation caused by overexpression of InR^{CA}. These changes included the number of EB cells, the pre-EE ratio in esg^+ cells, and a decrease in differentiated cells among total

Fig. 5 | Signaling pathway screening reveals downstream candidates responsible for ISC aging phenotype. a, b Quantification of the number of $esg^+NRE^-Pros^-$ ISCs (**a**) and NRE^+ EBs (**b**) per ROI in 10d flies with indicated genotypes. **c** The ratio of Pre-EE to total esg^+ cells per ROI in 10d flies with indicated genotypes. **d** The percentage of differentiated cells and esg^+ cells to total cells in 10d flies with indicated genotypes. **e, f** Quantification of the number of $esg^+NRE^-Pros^-$ ISCs (**e**) and NRE^+ EBs (**f**) per ROI in 40d flies with indicated genotypes. The dark dotted line represents the mean value from 10d control flies. **g** The ratio of Pre-EE to total esg^+ cells per ROI in 40d flies with indicated genotypes. The dark dotted line represents the mean value from 10d control flies. **h** The percentage of differentiated cells and esg^+ cells to total cells in 40d flies with indicated genotypes. The purple line represents the mean percentage value of differentiated cells from 10d control flies. The green line

represents the mean percentage value of esg^+ cells from 10d control flies. **i** The percentage of ECs and EEs to total differentiated cells in 40d flies with indicated genotypes. The red line represents the mean percentage value of ECs from 10d control flies. The blue line represents the mean percentage value of EEs from 10d control flies. ROI size 84,100 μm^2. For dot plots, bars are mean ± SD. For box plots, box shows median, 25th and 75th percentiles and whiskers represent minima and maxima. Each group was compared to the control group in all analyses. Statistics were measured by one-way ANOVA. Each dot represents one ROI in (**a**–**c**) and (**e**–**g**). From left to right, $n = 18, 9, 12, 15, 17, 15, 12, 17, 16, 23, 30, 16$ and 25, respectively in (**a**–**d**), $n = 18, 13, 32, 21, 38, 42, 19, 29$ and 24, respectively, in (**e**–**g**) and $n = 18, 13, 32, 21, 27, 33, 19, 29$ and 24, respectively, in (**h**-**i**). Source data are provided as a Source Data file.

epithelial cells (Fig. 7f–i, k–m), but not the number of ISCs or the percentage of ECs among differentiated cells (Fig. 7j and Supplementary Fig. 15o). These data suggested that SOX21A functions as a downstream of InR signaling.

Together, our data suggest that the InR signaling functions upstream of the RAB7-SOX21A axis to regulate the age-associated changes in *Drosophila* ISC differentiation direction.

RAB7 is down-regulated in ISCs of humans during aging

To investigate the conservation of mechanisms governing ISC differentiation direction through RAB7-mediated endocytosis during aging between *Drosophila* and humans, we tested the number of the late endosomes (marked by RAB7) in human ISCs (marked by SOX9) by immunofluorescence staining. In the duodenum of older individuals, ISCs displayed a reduced number of late endosomes compared to ISCs in younger individuals (Fig. 8a–c). These results suggest the existence of conserved mechanisms that regulate ISC differentiating direction between *Drosophila* and humans (Fig. 8d, e).

Discussion

Aging has become a growing global concern due to its impact on various biological processes. This study elucidated how nutrient-sensing pathways contribute to changes in intestinal stem cell differentiation direction during aging (Fig. 8). Specifically, we discovered that the RAB7-SOX21 axis, to some extent, regulates ISC differentiation direction as a downstream component of the nutrient-sensing pathway.

Notably, we noticed that in previous reports, the ISC number increases in *Drosophila* but decreases in mammals upon aging[20]. This discrepancy could be attributed to the imprecise identification of ISC solely by the Dl$^+$ marker in *Drosophila*. Dl$^+$ markers predominantly identify active ISCs, while quiescent ISCs still constitute a substantial population within the epithelium even under aging conditions. In this study, we used $esg^+NRE^-Pros^-$ to label ISCs, which did not exhibit a robust increase in ISC numbers during aging or under various genetic manipulations (Figs. 2–7). These findings align more closely with observations in mammals, suggesting that our strategy should be prioritized for studying ISCs in *Drosophila*.

Employing this method, we identified a conservative shift in ISC differentiation towards increased secretory lineage during aging across *Drosophila*, mouse and human (Figs. 1 and 2). Recently, there have been reports indicating that aging in *Drosophila* leads to an increase in ISC-to-enteroendocrine (EE) differentiation[60]. In our study, we further confirmed the functional changes occurring in the intestine as evidenced by a decreased ratio of enterocytes (ECs) and a reduction in the expression levels of EC-specific enzymes (Fig. 2). Importantly, our 3D organoid culture data align with these findings, revealing an elevated presence of differentiated Paneth cells and enteroendocrine cells in organoids derived from aged mice (Fig. 1). These observations suggest that there are conservative changes in ISC differentiation. Morevoer, we proved that in *Drosophila*, the evaluation of esg^+ cells predominantly comprised of EBs and pre-EEs, but not ISCs (Fig. 2).

Specifically, compared with 10-day-old flies, 30-day-old flies exhibited a 3.7-fold increase in EB number (Supplymentary Fig. 2a) but over a 10-fold in crease in pre-EE number (Fig. 2f). These results support the idea of a shift in ISC differentiation towards secretory lineage. Also, these shed light on the age-related changes to be failure of EB-to-EC differentiation and subsequently deregulation of ISC-to-pre-EE differentiation.

Previous studies have indicated that nutrient-sensing pathways undergo dysregulation under conditions of obesity or aging[59,61]. While the role of nutrient-sensing pathways in regulating stem cell proliferation has been highlighted[40], little is known about whether and how they influence stem cell differentiating direction. Using the *Drosophila* midgut system as a model, our study demonstrates the essential role of the nutrient-sensing pathway in mediating changes in intestinal stem cell differentiating direction mediated by HSD or aging. Specifically, upregulating the activity of the InR signaling pathway in young wild-type flies is sufficient to increase ISC-to-EE differentiation (Fig. 2). Conversely, downregulation of the InR signaling pathway effectively counteracts the abnormal changes in stem cell differentiation direction and cellular components within the intestinal epithelium (Fig. 3).

The transcription factor SOX21A has been implicated in the regulation of ISC-to-EC differentiation in *Drosophila*[53,54]. Meanwhile, our previous report demonstrated the crucial role of the RAB7-SOX21A axis in governing ISC-to-EC differentiation in response to injury[56]. However, it remains unclear whether the RAB7-SOX21A axis also regulates ISC differentiating direction. Here, we made significant discoveries in *Drosophila*, showing that depletion of either RAB7 (Fig. 5) or SOX21A (Supplementary Fig. 15a–d) in the ISCs of young flies is sufficient to alter ISC differentiating direction. Force expression of RAB7^{CA} or SOX21A in ISCs of aged flies attenuates the deregulated differentiating direction mediated by aging (Fig. 5). Despite the higher expression of SOX21A in EBs leading to no reduction in its levels when knocked down in ISCs, overexpressing SOX21A in ISCs elevated its expression levels and still alleviated the aging-mediated directional deregulation in differentiation. We also proved that both RAB7[57] and SOX21A (Fig. 7) are down-regulated during aging. Furthermore, genetic analysis revealed that the RAB7-SOX21A axis functions downstream of the InR signaling pathway to regulate ISC differentiating direction (Figs. 6 and 7). Finally, our findings extend beyond *Drosophila*, as human samples also showed a decreased amount of RAB7-labeled late endosomes in SOX9$^+$ ISCs aged individuals (Fig. 8). This highlights the functional conservation of the RAB7-SOX21 axis in regulating ISC differentiating direction.

Previous report uncovered the mechanisms regulating ISC differentiating direction through the Scute/Asense expression negative feedback loop[58]. Inspired by these findings, we propose a model that the deregulation of the nutrient-sensing pathway alters the activity of the RAB7-SOX21A axis in ISCs, inhibiting ISC-to-EC differentiation. Due to the feedback loop, ISCs present increased ISC-to-EE differentiation (Fig. 8). These underlying mechanisms may
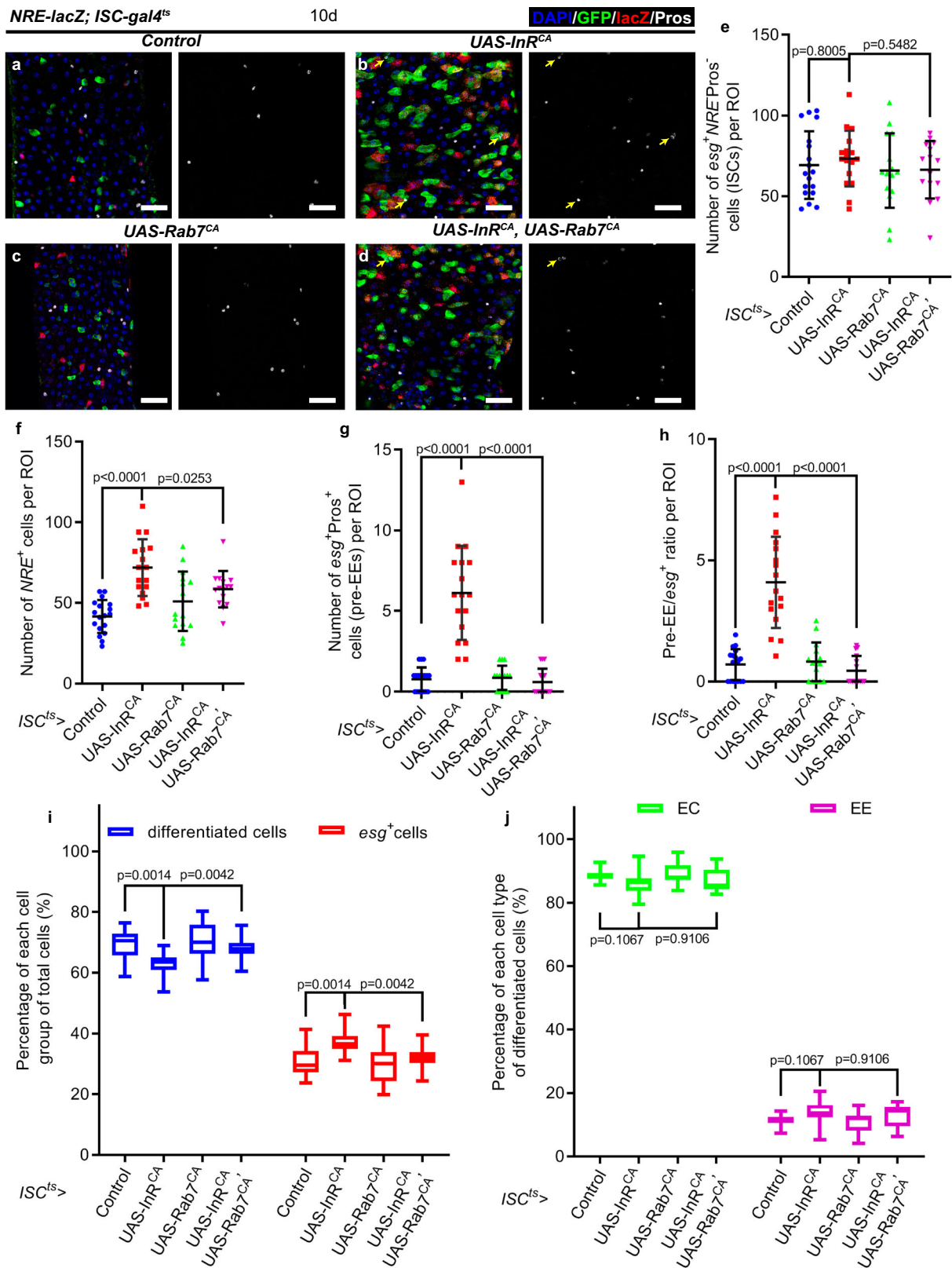
Fig. 6 | RAB7 regulates ISC differentiating direction downstream of InR.
a–d Representative immunofluorescence images of midguts with ISC-GFP (green), NRE-lacZ (red) and Pros (white) staining from 10d flies expressing *UAS-GFP* (used as control, **a**), *InR^CA* (**b**), *Rab7^CA* (**c**), and *InR^CA, Rab7^CA* (**d**) in driven by *ISC^ts-Gal4*. **e–g** Quantification of the number of esg^+NRE^-Pros$^-$ ISCs (**e**), NRE^+ EBs (**f**) and esg^+Pros$^+$ pre-EEs (**g**) per ROI of midguts in experiments (**a–d**). **h** The ratio of pre-EE cells to esg^+ cells per ROI with indicated genotypes of midguts in experiments (**a–d**). **i** The percentage of differentiated cells and esg^+ cells to total cells per ROI in indicated genotypes of midguts in experiments (**a–d**). **j** The percentage of ECs and EEs to total differentiated cells in indicated genotypes of midguts in experiments (**a–d**). ROI size 84,100 μm². DAPI-stained nuclei (blue). Yellow arrows indicate esg^+Pros$^+$ pre-EE cells. Scale bar, 25 μm. For dot plots, bars are mean ± SD. For box plots, box shows median, 25th and 75th percentiles and whiskers represent minima and maxima. Statistics were measured by one-way ANOVA. Each dot represents one ROI in (**e–h**). From left to right, $n = 18, 17, 15$, and 15, respectively in (**e–j**). Source data are provided as a Source Data file.

contribute to the observed phenotypes in aged human individuals and aging flies. However, our investigation still has limited insights into how the nutrient-sensing pathway precisely regulates RAB7 in ISCs. Given that recent research has shed light on the degradation of InR via the endocytosis pathway in hepatocytes upon insulin stimulation[62]. This hinted at the potential mechanisms by which the nutrient-sensing pathway regulates RAB7 in ISCs since blood insulin levels are elevated in obese and aging individuals, and Further research is required to investigate the above hypothesis.

Notably, the above discussion about InR-RAB7-SOX21A axis is likely to be part of mechanisms of ISC aging. We demonstrated that the TOR signaling and the Notch signaling also function downstream of InR signaling pathway (Supplymentary Figs. 13 and 14). This highlights the complexity of aging and that age-related changes cannot be simply explained by any single factors. Therefore, more investigations should be addressed on this field.

Methods

Ethical regulation statement

For human samples, the study protocol complied with the ethical guidelines of the 1975 Declaration of Helsinki principles and was approved by the Human Ethics Committee of West China Hospital, Sichuan University in 2020 with a document numbered 137.

For mice, animal ethical and welfare was approved by West China Hospital, Sichuan University in 2023 in a document numbered 20230209007.

Human samples

Human intestinal tissues from patients were provided by Doctor Yi Chen of West China Hospital, Sichuan University. The intestinal tissues were collected from 36 participants with no disease diagnosis at West China Hospital, Sichuan University between April 2022 and October 2022 (see Table 1 and Source Data of Fig. 1 for participant information). The gut samples were checked on the day of surgery and mucosal biopsies were ensured during endoscopy. Tissue segments were resected during surgery. All participants provided written informed consent for this study. No participant compensation was reported.

Twenty duodenum samples and 12 jejunum samples from 32 participants were finally used. Source Data of Fig. 1 includes gender and age of each participant. Sex and/or gender was not considered in study design. The gender of participants was determined based on self-report.

Drosophila stocks

The fly stocks used in this study are listed in Supplementary Data 1. The full genotypes of flies as they appear in each figure panel are listed in Supplementary Data 2.

Drosophila husbandry

All flies were cultured at 25 °C at a 12 h light/dark cycle. For the Gal4/Gal80ts system, the parents were crossbred at 18 °C to produce progeny. After eclosion, the offspring were still kept at 18 °C for 5 days or 35 days to allow Gal80ts to repress Gal4. Then flies were shifted to 29 °C removing Gal80 inhibition and enabling Gal4 to drive UAS-linked transgene expression. For MARCM and G-Trace system, all the time flies were raised at 20 °C for 10 days or 30 days.

Except for flies for special diet experiments, all flies were cultured on the standard cornmeal and yeast fly food with the recipe: 1 L H_2O, 50 g cornmeal, 12.5 g yeast, 61.7 g sucrose, 48.3 g glucose, 6.7 g agar, 0.55 g $CaCl_2$, and 6.7 mL propionic acid. Food for diet restriction experiment was made with the following protocal: 1 L H_2O, 50 g cornmeal, 6.25 g yeast (half of the standard food), 61.7 g sucrose, 48.3 g glucose, 6.7 g agar, 0.55 g $CaCl_2$, and 6.7 mL propionic acid. High-sugar food was prepared with the recipe: 1 L H_2O, 50 g cornmeal, 25.0 g yeast, 370 g sucrose, 48.3 g glucose, 6.7 g agar, 0.55 g $CaCl_2$, and 6.7 mL

propionic acid. Food for 100 mM methionine supplement experiment was made with the following protocal: 1 L H_2O, 50 g cornmeal, 12.5 g yeast, 61.7 g sucrose, 48.3 g glucose, 6.7 g agar, 0.55 g $CaCl_2$, 14.921 g methionine and 6.7 mL propionic acid. Food for 100 mM leucine supplement experiment was made with the following protocal: 1 L H_2O, 50 g cornmeal, 12.5 g yeast, 61.7 g sucrose, 48.3 g glucose, 6.7 g agar, 0.55 g $CaCl_2$, 13.118 g leucine and 6.7 mL propionic acid. Food for 200 μM rapamycin supplement experiment was made with the following protocal: 1 L H_2O, 50 g cornmeal, 12.5 g yeast, 61.7 g sucrose, 48.3 g glucose, 6.7 g agar, 0.55 g $CaCl_2$, 182.834 mg rapamycin and 6.7 mL propionic acid.

Bleomycin treatment

Drosophila were transferred from the medium to empty bottles for 2 h. The filter paper was cut into 3.5 × 6.0 cm pieces and treated with 5% (wt/vol) sucrose with 25 μg/mL bleomycin (BLM). Then, the moist papers were added to empty bottles for 24 h, and Drosophila were transferred into a new standard medium without BLM for another 24 h before dissection. Identical Drosophila fed 5% sucrose were used as control.

Immunofluorescence microscopy

Adult mated female fly intestines were dissected in 4 °C PBS and then fixed with 100 μl 4% EM-grade paraformaldehyde fixation buffer and 100 μl n-Heptane for 20 min. All intestines were washed in 200 μl methanol for 2 times, 5 min each. They were subsequently rinsed in 200 μl PBS plus 0.1% Triton X-100 (Sigma, PBST) for 2 times, 5 min each. The tissues were then incubated with primary antibodies dissolved in 0.1% PBST for overnight at 4 °C. Then they were washed with 0.1% PBST for 3 times, 5 min each before secondary antibodies and DAPI (1:1000; Sigma) incubated for 2 h at room temperature. After secondary antibodies incubation, the intestines were washed with 0.1% PBST for 3 times, 5 min each. The sources and dilutions of antibodies used are listed as follows: Chicken anti-GFP (1:1000; ab13970, Abcam), Rabbit anti-GFP (1:1000; 50430-2-AP, Proteintech), Mouse anti-GFP (1:1000; PA1-24030005, GENE CREATE), Rabbit SOX9 antibody (1:50, CY5400, Abways TECHOLOGY), Rab7 antibody (1:40, DSHB), Chicken anti-β-Galactosidase (1:1000; ab9361, Abcam), Rabbit anti-HA (1:1000; 3724, Cell signaling Technology), pAkt antibody (1:100; 4060, Cell signaling Technology), p4E-BP1 antibody (1:500; #2855, Cell signaling Technology), Rabbit anti-phosphoHistone H3 (ser10) (Millipore; Cat# 06-570); Prospero antibody (1:200; MR1A, DSHB), Delta antibody, (1:50; C594,9B, DSHB), Armadillo antibody (1:50; N2 7A1, DSHB), and Alexa Fluor secondary antibodies (1:2000; A11004, A11008, A11011, A11039, A32733, A-11041, A-11001, A-21235 and A32933). Leica TCS-SP8 (Laika, v3.5.5.19976) confocal microscope were used to acquire all immunofluorescence images. For each set of experiments, images were acquired as confocal stacks using the same settings.

Mice husbandry

Eight-week-old and 18-20-month-old male C57BL/6 mice were given ad libitum access to standard food before being sacrificed. Mice were housed in groups of five animals and maintained at 23 ± 1 °C and 45–65% humidity on a 12-h dark/light cycle. At West China Hospital, Sichuan University, all mice were housed in the Vivarium, and their care was monitored by the Experimental Animal Center under the Institutional Animal Care following committee protocol GB/T 35892-2018.

Organoid culture

Mouse small intestines were flushed with cold PBS and opened laterally. Villi were scraped off gently with a glass slide. The remaining tissue was cut into 1-2 mm sections. Intestine pieces were rinsed several times and incubated at 4 °C in 5 mM EDTA/PBS for 50-60 min. Subsequently, crypts were collected by mechanical shaking and filtered through a 70-μm mesh to remove villous fragments. Isolated
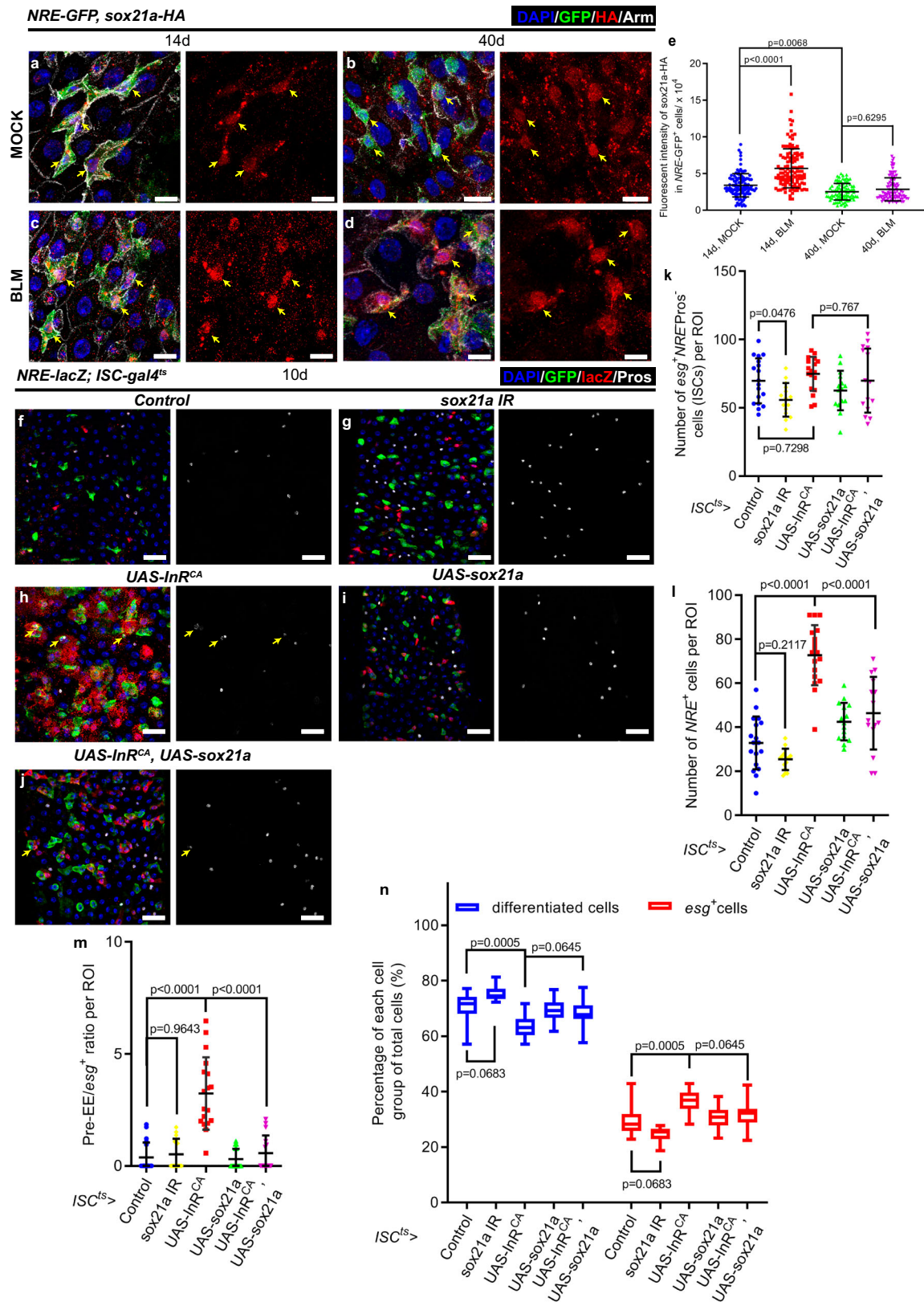
crypts were counted and embedded in 1:1 media: Matrigel (BD bioscience 356230, growth factor reduced) mixture at 500 crypts per 50 µl and cultured in a crypt culture medium. Unless otherwise described, crypts were grown in mixed Advanced DMEM/F12 (Gibco, 12634010) and GlutaMAX (31980030, 12491015) supplemented with EGF 50 ng/ml (Peprotech, 315-09), Noggin 100 ng/ml (Peprotech 250-38), R-Spondin 500 ng/ml (Peprotech, 120-38), N-acetyl-L-cysteine 1 mM (Sigma Aldrich, A7250), B27 50x (Gibco, 17504044), N2 100x (Gibco, 17502001). Intestinal crypts were plated in 50 µl droplets of Matrigel and placed on flat-bottomed 24-well plates and allowed to solidify for 10-15 min in a 37 °C incubator. 500 µL of crypt medium was added to each well and maintained at 37 °C in a humidified incubator at 5% CO_2. The crypt medium was changed every three days. For immunofluorescence, organoids were removed from Matrigel and fixed for

Fig. 7 | SOX21A is down-regulated in aged flies and functions downstream of InR. a–d Representative immunofluorescence images of midguts from 14d flies (*NRE-GFP; Sox21a-HA*) without BLM treatment (as mock, **a**), 40d flies without BLM treatment (**b**), 14d flies treated with BLM (**c**), and 40d flies treated with BLM (**d**). SOX21A was labeled by HA (red). Armadillo (Arm, white) labeled plasma membrane. Yellow arrows indicate EBs. **e** Quantification of fluorescent intensity of SOX21A-HA in *NRE*-GFP⁺ EBs of midguts of experiments (**a-d**). Each dot represents one *NRE*-GFP⁺ EB. From left to right, $n = 107$, 119, 90, and 98, respectively. **f–j** Representative immunofluorescence of midguts with ISC-GFP (green), NRE-lacZ (red) and Pros (white) staining from 10d flies expressing *UAS-GFP* (used as control, **f**), *UAS-sox21a RNAi* (**g**), *UAS-InR^CA* (**h**), *UAS-sox21a* (**i**), and *UAS-sox21a, UAS-InR^CA* (**j**) driven by *ISC^ts-*

Gal4. Yellow arrows indicate *esg*⁺Pros⁺ pre-EE cells. **k–l** Quantification of the number of *esg*⁺*NRE*⁻Pros⁻ ISCs (**k**) and *NRE*⁺ EBs (**l**) per ROI with indicated genotypes of midguts in experiments (**f–j**). **m** The ratio of pre-EE to total *esg*⁺ cells per ROI with indicated genotypes of midguts in experiments (**f–j**). **n** The percentage of differentiated cells and *esg*⁺ cells to total cells with indicated genotypes of midguts in experiments (**f–j**). DAPI-stained nuclei (blue). Scale bar, 10 μm in (**a–d**) and 25 μm in (**f–j**). For dot plots, bars are mean ± SD. For box plots, box shows median, 25th and 75th percentiles and whiskers represent minima and maxima. Statistics were measured by one-way ANOVA. Each dot represents one ROI in (**k–n**). From left to right, $n = 18$, 15, 18, 15, and 15, respectively in (**k–n**). Source data are provided as a Source Data file.
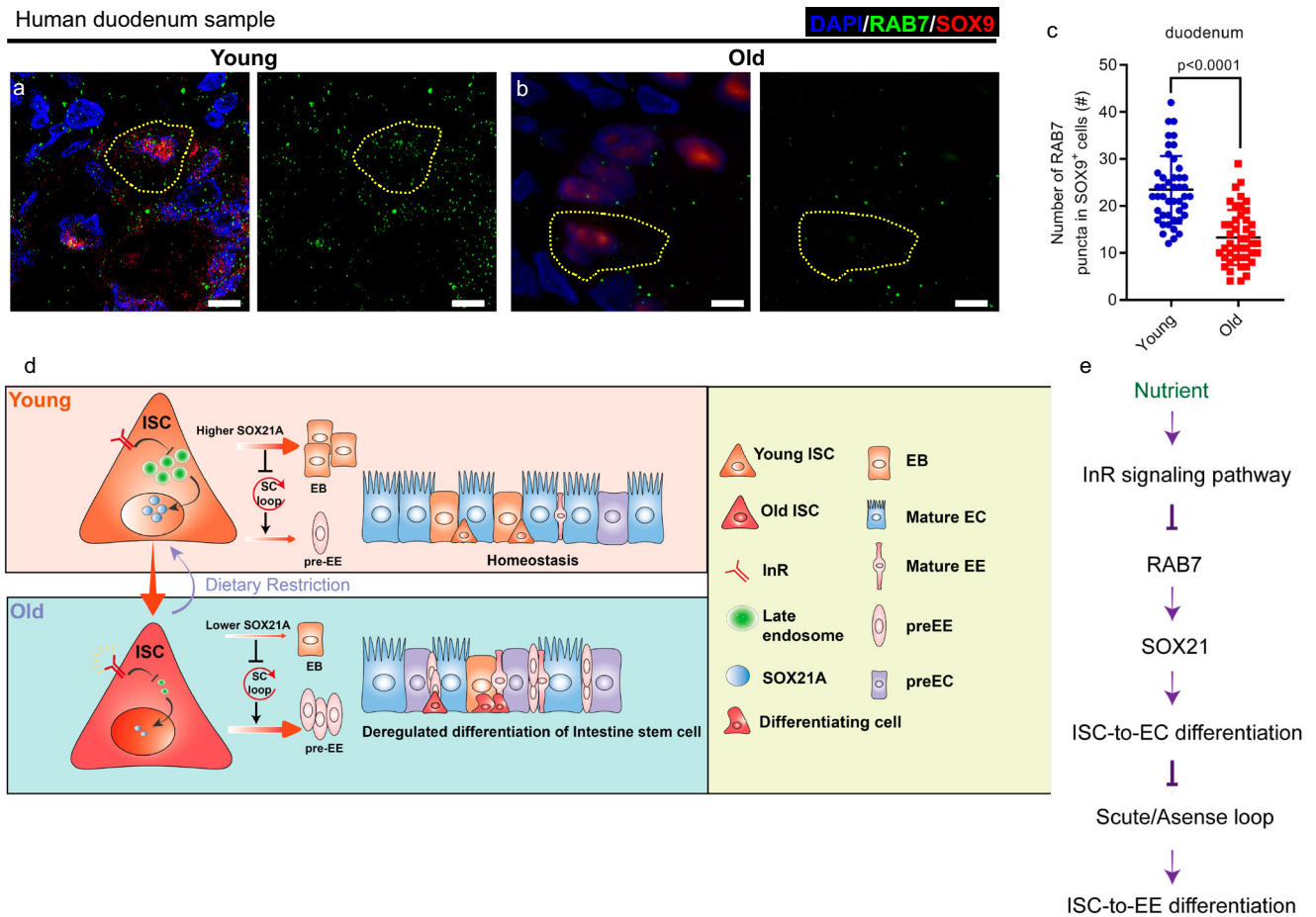
Fig. 8 | RAB7 is down-regulated in aged human ISCs. a, **b** Immunofluorescence images of human duodenum samples section with RAB7 (green) and SOX9 (red) staining from young (**a**) and old (**b**) groups. **c** Quantification of the number of RAB7⁺ endosomes in SOX9-labeled ISCs of human samples from the young group ($n = 45$) and the old group ($n = 45$). Each dot represents one SOX9⁺ ISC. **d**, **e** Schematic of the proposed model. InR is aberrantly upregulated in ISCs upon aging, which leads to

reduced differentiation into ECs through the down-regulating RAB7-SOX21A axis. Due to the SC loop, ISCs exhibit a change of differentiating direction. DAPI-stained nuclei (blue). Yellow frames indicate SOX9⁺ ISCs. Scale bar, 5 μm. Bars are mean ± SD. Statistics were measured by two-tailed, unpaired student's *t*-test. Source data are provided as a Source Data file.

30 min in 4% PFA/PBS at room temperature. Subsequently, samples were permeabilized with 0.2% Triton X-100 (Sigma) in PBS (1 h, RT). Organoids were then incubated overnight at 4 °C with anti-Lysozyme (1:1000; DAKO, A0099) and anti-Chromogranin-A (1:500; Santa Cruz, sc-393941). After washing, samples were incubated for 2 h at room temperature with secondary antibodies. Samples were then washed and imaged.

Immunofluorescence and immunohistochemistry for mammalian tissues

Samples were fixed in 4% (w/v) paraformaldehyde for 48 h. After sectioned, they were baked at 65 °C for 30 min, then biotransparent was

used for 30 min. Sections were then washed with sequential gradient over anhydrous ethanol, 95% ethanol, 90% ethanol, 80% ethanol for 2-5 min each, followed with double-distilled water for 5 min. Citrate was used for microwave antigen repair, followed by washing with PBS for 5 min twice.

For immunofluorescence, after blocking with 5% serum for 30 min, primary antibody (anti-SOX9, 1:1000, Abcam, ab185966; anti-RAB7, 1:200, Abcam, ab137029) was added and incubated at 4 °C overnight. After washing with PBS for 5 min, 3 times, secondary antibody and DAPI were added and incubated at room temperature for 2 h. Samples were then washed and imaged.

Table 1 | The demographic of all participants

Participant characteristics	Duodenum samples	Jejunum samples
Number of patients	22	14
Age, years (median, range)	38 (23–73)	39 (24–69)
Gender (male/female)	15/7	10/4

For immunohistochemistry, the sections were incubated with 3% H_2O_2 at room temperature for 30 min, followed by washing with double-distilled water. After blocking with 5% serum for 30 min, primary antibody (anti-ChgA, 1:400, Santa Cruz, sc-393941; anti-Lysozyme, 1:8000, DAKO, A0099; anti-DCAMKL1, 1:200, Abcam, ab31704; anti-Muc2, 1:100, Abcam, ab76774) was added and incubated at 4 °C overnight. After washing with TBST for 5 min, 3 times, biotin-conjugated secondary donkey anti-rabbit or anti-mouse antibodies (Abcam) were added and incubated at 37 °C temperature for 1 h. The Vectastain Elite ABC immunoperoxidase detection kit (Vector Labs, PK-6101) followed by Dako Liquid DAB+ Substrate (Dako) was used for visualization.

For Alcian blue staining and TUNEL staining, Alcian blue 8GX (Sgima, A5268) and TUNEL assay kit (Abcam, ab66110) were used and experiments were performed based on the protocols provided by the manufacturer.

RNA isolation and RT-qPCR
50 adult midguts were dissected or all cultured organoids were collected into 4 °C diethylpyrocarbonate (DEPC)-treated water-PBS solution. Samples were homogenized in RNA-easy Isolation Reagent (Vazyme, R701) for total RNA isolation and cDNA synthesis. RT-qPCR was performed on a CFX96 Touch Deep Well (Bio-Rad) using ChamQ Universal SYBR qPCR Master Mix (Vazyme, Q711). The reference standard group was Rp49 for *Drosophila* samples and GAPDH for mice organoid samples. The expression levels were counted by the $2^{-\triangle\triangle CT}$ method. The expression level of the control sample was normalized to 1.0. The primers used were listed in Supplementary Data 3.

Western blot analysis
For western blotting, samples were isolated from young and old small intestinal crypts. The primary antibodies used for western blotting in this study were: anti-p4E-BP1 (rabbit, 1:1000, Cell signaling Technology, Cat#2855); and anti-GAPDH (rabbit, 1:2000, Cell Signaling Technology, Cat# 2118). The secondary antibody was horseradish peroxidase-conjugated goat anti-rabbit (1:5000, Jackson ImmunoResearch Labs, Cat# 211-032-171).

Fluorescence intensity statistics
Immunofluorescence imaging results were analyzed based on z-stacks acquired with confocal microscopy. The fluorescence intensity of the region of interest (ROI) or cell was calculated using ImageJ software following the fomular:

$$\begin{aligned} \text{Integrated Density} = \text{Integrated Density of ROI or cell} \\ - \text{Integrated Density of background region}/ \\ \text{Area of background region} \times \text{Area of ROI or cell}. \end{aligned}$$

Statistics and reproducibility
Data were statistically analyzed using GraphPad Prism 7.0. For all experiments, data distribution was assumed to be normal, but this was not formally tested. All comparisons were done as two-sample comparisons or multiple sample camparisons and unpaired two-tailed t-test or one-way ANOVA was used to determine significance. *P* values are indicated on dot plots and box-and-whisker plots. For dot plots, data were presented as mean ± SD. For box-and-whisker plots, horizontal lines inside boxes indicate medians, box edges represent 25th and 75th percentiles, and whiskers extend to minima and maxima. For all experiments, no statistical methods were used to predetermine sample size, but our sample sizes are similar to those reported in previous literature[31,60].

No randomization method was used to allocate animals to experimental groups. The investigators were not blinded during data collection or analyses. Blinding during data collection was not possible for mouse studies since the experimental conditions caused noticeable phenotypic differences among the groups (old versus young). Blinding during data analysis was not relevant in most cases because automated analysis software was used uniformly.

Reporting summary
Further information on research design is available in the Nature Portfolio Reporting Summary linked to this article.

Data availability
All data presented are available in the main text or the supplementary materials. The data set generated and/or analyzed during this study is available with no restrictions. Source data are provided with this paper.

References
1. Fontana, L., Partridge, L. & Longo, V. D. Extending healthy life span—from yeast to humans. *Science* **328**, 321–326 (2010).
2. Hotamisligil, G. S. & Erbay, E. Nutrient sensing and inflammation in metabolic diseases. *Nat. Rev. Immunol.* **8**, 923–934 (2008).
3. Micó, V., Berninches, L., Tapia, J. & Daimiel, L. NutrimiRAging: micromanaging nutrient sensing pathways through nutrition to promote healthy aging. *Int. J. Mol. Sci.* **18**, 915 (2017).
4. Post, Y. & Clevers, H. Defining adult stem cell function at its simplest: the ability to replace lost cells through mitosis. *Cell Stem Cell* **25**, 174–183 (2019).
5. Ji, J. et al. Aging in hair follicle stem cells and niche microenvironment. *J. Dermatol.* **44**, 1097–1104 (2017).
6. Yamakawa, H., Kusumoto, D., Hashimoto, H. & Yuasa, S. Stem cell aging in skeletal muscle regeneration and disease. *Int. J. Mol. Sci.* **21**, 1830 (2020).
7. Foster, D. A., Yellen, P., Xu, L. & Saqcena, M. Regulation of G1 cell cycle progression: distinguishing the restriction point from a nutrient-sensing cell growth checkpoint(s). *Genes Cancer* **1**, 1124–1131 (2011).
8. Fidaleo, M., Cavallucci, V. & Pani, G. Nutrients, neurogenesis and brain ageing: From disease mechanisms to therapeutic opportunities. *Biochem. Pharmacol.* **141**, 63–76 (2017).
9. Easley, C. A. et al. mTOR-mediated activation of p70 S6K induces differentiation of pluripotent human embryonic stem cells. *Cell. Reprogramming* **12**, 263–273 (2010).
10. Oñate, B. et al. The subcutaneous adipose tissue reservoir of functionally active stem cells is reduced in obese patients. *FASEB J.* **26**, 4327–4336 (2012).
11. Meier, B. & Burton, J. H. Myeloproliferative disorders. *Hematol./Oncol. Clin. North Am.* **31**, 1029–1044 (2017).
12. Inaba, H. & Mullighan, C. G. Pediatric acute lymphoblastic leukemia. *Haematologica* **105**, 2524–2539 (2020).
13. de Haan, G. & Lazare, S. S. Aging of hematopoietic stem cells. *Blood* **131**, 479–487 (2018).
14. Florian, M. C. et al. A canonical to non-canonical Wnt signalling switch in haematopoietic stem-cell ageing. *Nature* **503**, 392–396 (2013).
15. Challen, G. A., Boles, N. C., Chambers, S. M. & Goodell, M. A. Distinct hematopoietic stem cell subtypes are differentially regulated by TGF-β1. *Cell Stem Cell* **6**, 265–278 (2010).

16. Beerman, I. et al. Proliferation-dependent alterations of the DNA methylation landscape underlie hematopoietic stem cell aging. *Cell Stem Cell* **12**, 413–425 (2013).

17. Ho, Y.-H. et al. Remodeling of bone marrow hematopoietic stem cell niches promotes myeloid cell expansion during premature or physiological aging. *Cell Stem Cell* **25**, 407–418.e406 (2019).

18. Wei, Q. & Frenette, P. S. Niches for hematopoietic stem cells and their progeny. *Immunity* **48**, 632–648 (2018).

19. Nászai, M., Carroll, L. R. & Cordero, J. B. Intestinal stem cell proliferation and epithelial homeostasis in the adult Drosophila midgut. *Insect Biochem. Mol. Biol.* **67**, 9–14 (2015).

20. Jasper, H. Intestinal stem cell aging: origins and interventions. *Annu. Rev. Physiol.* **82**, 203–226 (2020).

21. Ohlstein, B. & Spradling, A. The adult Drosophila posterior midgut is maintained by pluripotent stem cells. *Nature* **439**, 470–474 (2005).

22. Micchelli, C. A. & Perrimon, N. Evidence that stem cells reside in the adult Drosophila midgut epithelium. *Nature* **439**, 475–479 (2005).

23. Ohlstein, B. & Spradling, A. Multipotent drosophila intestinal stem cells specify daughter cell fates by differential notch signaling. *Science* **315**, 988–992 (2007).

24. Guo, Z. & Ohlstein, B. Bidirectional Notch signaling regulates Drosophila intestinal stem cell multipotency. *Science* **350**, https://doi.org/10.1126/science.aab0988 (2015).

25. Lin, X. & Smagghe, G. Roles of the insulin signaling pathway in insect development and organ growth. *Peptides* **122**, 169923 (2019).

26. Owusu-Ansah, E. & Perrimon, N. Modeling metabolic homeostasis and nutrient sensing in Drosophila: implications for aging and metabolic diseases. *Dis. Models Mechanisms* **7**, 343–350 (2014).

27. Choi, N. H., Lucchetta, E. & Ohlstein, B. Nonautonomous regulation of Drosophila midgut stem cell proliferation by the insulin-signaling pathway. *Proc. Natl Acad. Sci.* **108**, 18702–18707 (2011).

28. Rodriguez-Fernandez, I. A., Tauc, H. M. & Jasper, H. Hallmarks of aging Drosophila intestinal stem cells. *Mechanisms Ageing Dev.* **190**, 111285 (2020).

29. Chen, H., Zheng, X. & Zheng, Y. Age-associated loss of lamin-B leads to systemic inflammation and gut hyperplasia. *Cell* **159**, 829–843 (2014).

30. Kim, S. K. et al. Lifespan extension by preserving proliferative homeostasis in drosophila. *PLoS Genet.* **6**, e1001159 (2010).

31. Pentinmikko, N. et al. Notum produced by Paneth cells attenuates regeneration of aged intestinal epithelium. *Nature* **571**, 398–402 (2019).

32. Choi, N.-H., Kim, J.-G., Yang, D.-J., Kim, Y.-S. & Yoo, M.-A. Age-related changes in Drosophila midgut are associated with PVF2, a PDGF/VEGF-like growth factor. *Aging Cell* **7**, 318–334 (2008).

33. Minden, J. S., Agard, D. A., Sedat, J. W. & Alberts, B. M. Direct cell lineage analysis in Drosophila melanogaster by time-lapse, three-dimensional optical microscopy of living embryos. *J. cell Biol.* **109**, 505–516 (1989).

34. Harrison, D. A. & Perrimon, N. Simple and efficient generation of marked clones in Drosophila. *Curr. Biol.* **3**, 424–433 (1993).

35. Lee, T. & Luo, L. Mosaic analysis with a repressible cell marker for studies of gene function in neuronal morphogenesis. *Neuron* **22**, 451–461 (1999).

36. Evans, C. J. et al. G-TRACE: rapid Gal4-based cell lineage analysis in Drosophila. *Nat. Methods* **6**, 603–605 (2009).

37. Britton, J. S., Lockwood, W. K., Li, L., Cohen, S. M. & Edgar, B. A. Drosophila's insulin/PI3-kinase pathway coordinates cellular metabolism with nutritional conditions. *Dev. Cell* **2**, 239–249 (2002).

38. Huang, X., Liu, G., Guo, J. & Su, Z. The PI3K/AKT pathway in obesity and type 2 diabetes. *Int. J. Biol. Sci.* **14**, 1483–1496 (2018).

39. Dragojlovic-Munther, M. & Martinez-Agosto, J. A. Multifaceted roles of PTEN and TSC orchestrate growth and differentiation of Drosophila blood progenitors. *Development* **139**, 3752–3763 (2012).

40. Ochocki, J. D. & Simon, M. C. Nutrient-sensing pathways and metabolic regulation in stem cells. *J. Cell Biol.* **203**, 23–33 (2013).

41. Clancy, D. J. et al. Extension of life-span by loss of CHICO, a drosophila insulin receptor substrate protein. *Science* **292**, 104–106 (2001).

42. Green, C. L., Lamming, D. W. & Fontana, L. Molecular mechanisms of dietary restriction promoting health and longevity. *Nat. Rev. Mol. Cell Biol.* **23**, 56–73 (2021).

43. Partridge, L., Piper, M. D. W. & Mair, W. Dietary restriction in Drosophila. *Mechanisms Ageing Dev.* **126**, 938–950 (2005).

44. Zhang, X., Jin, Q. & Jin, L. H. High sugar diet disrupts gut homeostasis though JNK and STAT pathways in Drosophila. *Biochem. Biophys. Res. Commun.* **487**, 910–916 (2017).

45. Anzelon, A. N., Wu, H. & Rickert, R. C. Pten inactivation alters peripheral B lymphocyte fate and reconstitutes CD19 function. *Nat. Immunol.* **4**, 287–294 (2003).

46. Choorapoikayil, S., Kers, R., Herbomel, P., Kissa, K. & den Hertog, J. Pivotal role of Pten in the balance between proliferation and differentiation of hematopoietic stem cells in zebrafish. *Blood* **123**, 184–190 (2014).

47. Doupé, D. P., Marshall, O. J., Dayton, H., Brand, A. H. & Perrimon, N. Drosophila intestinal stem and progenitor cells are major sources and regulators of homeostatic niche signals. *Proc. Natl Acad. Sci.* **115**, 12218–12223 (2018).

48. Biteau, B. & Jasper, H. EGF signaling regulates the proliferation of intestinal stem cells in Drosophila. *Development* **138**, 1045–1055 (2011).

49. Tian, A. & Jiang, J. Intestinal epithelium-derived BMP controls stem cell self-renewal in Drosophila adult midgut. *eLife* https://doi.org/10.7554/eLife.01857 (2014).

50. Nagy, P., Kovács, L., Sándor, G. O. & Juhász, G. Stem cell-specific endocytic degradation defects lead to intestinal dysplasia in Drosophila. *Dis. Models Mech.* https://doi.org/10.1242/dmm.023416 (2016).

51. Voog, J. et al. Escargot restricts niche cell to stem cell conversion in the drosophila testis. *Cell Rep.* **7**, 722–734 (2014).

52. Koehler, C. L., Perkins, G. A., Ellisman, M. H. & Jones, D. L. Pink1 and Parkin regulate Drosophila intestinal stem cell proliferation during stress and aging. *J. Cell Biol.* **216**, 2315–2327 (2017).

53. Zhai, Z. et al. Accumulation of differentiating intestinal stem cell progenies drives tumorigenesis. *Nat. Commun.* https://doi.org/10.1038/ncomms10219 (2015).

54. Barsh, G. S. et al. A genetic framework controlling the differentiation of intestinal stem cells during regeneration in Drosophila. *PLOS Genet.* **13**, e1006854 (2017).

55. Paling, N. R. D., Wheadon, H., Bone, H. K. & Welham, M. J. Regulation of embryonic stem cell self-renewal by phosphoinositide 3-kinase-dependent signaling. *J. Biol. Chem.* **279**, 48063–48070 (2004).

56. Du, G. et al. Peroxisome elevation induces stem cell differentiation and intestinal epithelial repair. *Dev. Cell* **53**, 169–184.e111 (2020).

57. Du, G. et al. Lipoic acid rejuvenates aged intestinal stem cells by preventing age-associated endosome reduction. *EMBO Rep.* https://doi.org/10.15252/embr.201949583 (2020).

58. Chen, J. et al. Transient Scute activation via a self-stimulatory loop directs enteroendocrine cell pair specification from self-renewing intestinal stem cells. *Nat. Cell Biol.* **20**, 152–161 (2018).

59. López-Otín, C., Blasco, M. A., Partridge, L., Serrano, M. & Kroemer, G. Hallmarks of aging: An expanding universe. *Cell* **186**, 243–278 (2023).

60. Tauc, H. M. et al. Age-related changes in polycomb gene regulation disrupt lineage fidelity in intestinal stem cells. *eLife* https://doi.org/10.7554/eLife.62250 (2021).

61. Dailey, M. J. Nutrient-induced intestinal adaption and its effect in obesity. *Physiol. Behav.* **136**, 74–78 (2014).

62. Liu, X. et al. Insulin induces insulin receptor degradation in the liver through EphB4. *Nat. Metab.* **4**, 1202–1213 (2022).

Author contributions

Conceptualization, Haiyang C.; Methodology, Z.Y., Y.Z., C.F., Z.Z., Y.Y., X.L., and Haiyang C.; Investigation, Z.Y., Y.Z., C.F., Z.Z., Y.Y., and X.L.; Writing-Original Draft, Z.Y., Y.Z., and Haiyang C.; Writing-Review & Editing, Z.Y., Y.Z., C.F., Z.Z., Haiou C., Y.Y., X.L., X.G, and Haiyang C.; Funding Acquisition, Haiyang C.; Resources, Haiou C., Haiyang C. and Y.C.; Supervision, Haiyang C.

Competing interests

The authors declare no competing interests.

Additional information

Supplementary information The online version contains supplementary material available at
https://doi.org/10.1038/s41467-024-53675-7.

Correspondence and requests for materials should be addressed to Haiyang Chen.

Peer review information *Nature Communications* thanks the anonymous reviewer(s) for their contribution to the peer review of this work. A peer review file is available.

Reprints and permissions information is available at http://www.nature.com/reprints

Publisher's note Springer Nature remains neutral with regard to jurisdictional claims in published maps and institutional affiliations.